AGU PUBLICATIONS

Paleoceanography

RESEARCH ARTICLE
10.1002/2015PA002863

Key Points:
- Little deep water circulation changes in the past 240,000 years in the central South Pacific
- Reduced North Atlantic Deep Water admixture during glacials to the Southern Ocean
- South Pacific lithogenic material mainly sourced from SE Australia and South New Zealand

Supporting Information:
- Supporting Information S1
- Table S1
- Table S2

Correspondence to:
M. Molina-Kescher,
mmolina-kescher@geomar.de

Citation:
Molina-Kescher, M., M. Frank, R. Tapia, T. A. Ronge, D. Nürnberg, and R. Tiedemann (2016), Reduced admixture of North Atlantic Deep Water to the deep central South Pacific during the last two glacial periods, *Paleoceanography*, *31*, 651–668, doi:10.1002/2015PA002863.

Received 22 JUL 2015
Accepted 19 MAY 2016
Accepted article online 23 MAY 2016
Published online 14 JUN 2016

Reduced admixture of North Atlantic Deep Water to the deep central South Pacific during the last two glacial periods

Mario Molina-Kescher[1], Martin Frank[1], Raúl Tapia[1], Thomas A. Ronge[2], Dirk Nürnberg[1], and Ralf Tiedemann[2]

[1]GEOMAR Helmholtz Centre for Ocean Research Kiel, Kiel, Germany, [2]Alfred Wegener Institute Helmholtz Zentrum für Polar- und Meeresforschung, Bremerhaven, Germany

Abstract The South Pacific is a sensitive location for the variability of the global oceanic thermohaline circulation given that deep waters from the Atlantic Ocean, the Southern Ocean, and the Pacific Basin are exchanged. Here we reconstruct the deep water circulation of the central South Pacific for the last two glacial cycles (from 240,000 years ago to the Holocene) based on radiogenic neodymium (Nd) and lead (Pb) isotope records complemented by benthic stable carbon data obtained from two sediment cores located on the flanks of the East Pacific Rise. The records show small but consistent glacial/interglacial changes in all three isotopic systems with interglacial average values of −5.8 and 18.757 for ε_{Nd} and $^{206}Pb/^{204}Pb$, respectively, whereas glacial averages are −5.3 and 18.744. Comparison of this variability of Circumpolar Deep Water (CDW) to previously published records along the pathway of the global thermohaline circulation is consistent with reduced admixture of North Atlantic Deep Water to CDW during cold stages. The absolute values and amplitudes of the benthic $\delta^{13}C$ variations are essentially indistinguishable from other records of the Southern Hemisphere and confirm that the low central South Pacific sedimentation rates did not result in a significant reduction of the amplitude of any of the measured proxies. In addition, the combined detrital Nd and strontium ($^{87}Sr/^{86}Sr$) isotope signatures imply that Australian and New Zealand dust has remained the principal contributor of lithogenic material to the central South Pacific.

1. Introduction

The global thermohaline circulation (THC) contributes to regulate Earth's climate through the redistribution of heat from lower to higher latitudes and also through transport and storage of nutrients, oxygen, and CO_2 in the deep ocean [e.g., *Broecker*, 1982; *Rahmstorf*, 2002; *Sigman et al*., 2010; *Adkins*, 2013]. The main deep water formation areas are located in the North Atlantic and in the Southern Ocean. Essentially, North Atlantic Deep Water (NADW) and Antarctic Bottom Water (AABW) mix with the eastward flowing Antarctic Circumpolar Current (ACC) in the Southern Ocean to form Circumpolar Deep Water (CDW), in which also deep waters of Pacific origin are entrained. CDW can be subdivided into nutrient-depleted Upper CDW (UCDW) and more nutrient-enriched Lower CDW (LCDW) [cf. *Carter et al*., 2009], which fill the deep Indian and Pacific Oceans via Deep Western Boundary Currents (DWBCs). Given that UCDW and LCDW cannot be distinguished based on their Nd isotope compositions, we only refer to CDW for the purpose of our study. The return flow to the Southern Ocean at middepths occurs via nutrient-rich and oxygen-depleted waters [e.g., *Kawabe and Fujio*, 2010]. The South Pacific represents the entrance and exit of deep water masses feeding and leaving the Pacific Ocean, which is the largest marine nutrient and CO_2 reservoir on Earth.

The carbon isotope composition ($\delta^{13}C$) of benthic foraminifera has been widely used to evaluate past changes in deep water circulation [*Boyle and Keigwin*, 1986; *Duplessy et al*., 1988; *Charles and Fairbanks*, 1992; *Sarnthein et al*., 1994; *Matsumoto and Lynch-Stieglitz*, 1999; *Matsumoto et al*., 2002; *Ninnemann and Charles*, 2002; *McCave et al*., 2008]. Its dissolved distribution follows the major nutrients in the present-day ocean and is overall consistent with the age and mixing of water masses along the thermohaline circulation. Young, nutrient-depleted water masses, such as NADW, are characterized by positive $\delta^{13}C$ values near +1‰, whereas the oldest, least ventilated deep water masses in the North Pacific are significantly lighter and even reach negative $\delta^{13}C$ signatures [*Lynch-Stieglitz*, 2003; *Ravelo and Hillaire-Marcel*, 2007]. The dissolved bottom water $\delta^{13}C$ signal can also be affected by processes other than water mass mixing, such as isotopic disequilibria between the atmosphere and the surface ocean [e.g., *Charles et al*., 1993], changes in primary production

[*Mackensen et al*., 1993], and the balance between terrestrial and oceanic carbon storage on glacial-interglacial time scales [*Oliver et al*., 2010; *Peterson et al*., 2014].

Radiogenic Nd isotope compositions ($^{143}Nd/^{144}Nd$) recorded in authigenic Fe-Mn coatings of sediment particles have been shown to reliably trace past deep circulation patterns unaffected by biological and thermodynamic fractionation effects [e.g., *Rutberg et al*., 2000; *Piotrowski et al*., 2004, 2005]. Water masses acquire their Nd isotope signal (expressed as $\varepsilon_{Nd} = [^{143}Nd/^{144}Nd_{(sample)}/^{143}Nd/^{144}Nd_{(CHUR)} - 1] \times 10^4$, whereby CHUR stands for the Chondritic Uniform Reservoir ($^{143}Nd/^{144}Nd = 0.512638$) [*Jacobsen and Wasserburg*, 1980]) in their formation areas as a consequence of weathering of continental rocks with distinct isotopic signatures. Consequently, deep water masses formed in the North Atlantic and spreading southward as NADW are characterized by a distinctly negative (unradiogenic) ε_{Nd} signature of approximately −13.5 [*Piepgras and Wasserburg*, 1987; *Rickli et al*., 2009; *Lambelet et al*., 2016], which originates from weathering of the old cratonic rocks of Canada and Greenland. In contrast, the ε_{Nd} signature of North Pacific Deep Water (NPDW) ranges from −2 to −4 [*Piepgras and Jacobsen*, 1988; *Amakawa et al*., 2004, 2009; *Horikawa et al*., 2011] due to the more positive (radiogenic) Nd isotope composition of the volcanic rocks that surround the Pacific [cf. *Jeandel et al*., 2007]. End-members from these main source areas mix in the Southern Ocean, resulting in ε_{Nd} signatures near −8.5 for CDW [*Piepgras and Wasserburg*, 1982; *Carter et al*., 2012; *Stichel et al*., 2012a; *Garcia-Solsona et al*., 2014; *Molina-Kescher et al*., 2014a]. Tracing the mixing of water masses along the thermohaline circulation pathway in the open ocean is possible due to the intermediate oceanic residence time of Nd of ~400–2000 years [*Tachikawa et al*., 2003; *Arsouze et al*., 2009; *Rempfer et al*., 2011], which is similar to the global ocean mixing time. In the water column of near-coastal regions, where Nd is introduced into seawater and in high-productivity areas with high particulate fluxes, dissolved Nd isotopes show nonconservative behavior that complicates or sometimes prevents their use as water mass tracers [*Lacan and Jeandel*, 2005; *Rempfer et al*., 2011; *Singh et al*., 2012; *Stichel et al*., 2012b; *Grasse et al*., 2012; *Pearce et al*., 2013]. This is, however, clearly not the case for the South Pacific, where the present-day dissolved Nd isotope compositions fully match the different deep and middepth water masses according to their hydrographic parameters, such as oxygen concentrations [*Molina-Kescher et al*., 2014a]. In addition, the reliable extraction of the authigenic, seawater-derived signature recorded in the sediments is sometimes hampered by easily dissolving volcanic particles or preformed coatings [*Gutjahr et al*., 2007; *Roberts et al*., 2010, 2012; *Elmore et al*., 2011; *Piotrowski et al*., 2012; *Wilson et al*., 2013; *Kraft et al*., 2013; *Tachikawa et al*., 2014]. For the South Pacific, including core top data for the cores of this study, *Molina-Kescher et al*. [2014b] comprehensively evaluated ε_{Nd} signatures from different sedimentary phases for their suitability to infer seawater Nd isotope compositions. Those data clearly documented that unclean foraminifera reliably recorded the authigenic signal. In addition, despite that the core locations of this study are on the slope of the East Pacific Rise, any hydrothermal influence on the Nd isotope signatures can be excluded based on the complete removal of hydrothermal Nd within the hydrothermal vents [*German et al*., 1990; *Halliday et al*., 1992], which even allows hydrothermal sediments to be used as archives for the Nd isotope composition of seawater [*Chavagnac et al*., 2006]. Also, the long distance of the study area from any continent or volcanic island makes contamination by volcanic ashes very unlikely.

Lead (Pb) isotopes behave similarly to Nd isotopes in seawater in that water masses from different oceanic basins present characteristic isotopic ratios as a consequence of the inputs from weathered continental rocks of different type and ages [cf. *Frank*, 2002]. In contrast to Nd isotopes, Pb isotopes undergo incongruent weathering resulting in the radiogenic Pb isotopes (^{206}Pb, ^{207}Pb, and ^{208}Pb) to be preferentially mobilized during weathering in comparison to primordial ^{204}Pb [*Chow and Patterson*, 1959, 1962; *Frank*, 2002]. In addition, hydrothermal inputs may play a role for local oceanic Pb budgets and the short residence time of Pb in seawater (~50 to 200 years) [*Schaule and Patterson*, 1981; *von Blanckenburg and Igel*, 1999] restricts its applicability to short-distance water mass mixing and tracing of lithogenic inputs. Nonetheless, differentiation of the admixture of deep water signatures from the Pacific and Atlantic to Circumpolar Deep Water (CDW) along its pathway is possible due to the very high current speeds and volume transport of the ACC [*Abouchami and Goldstein*, 1995].

The long residence time of Sr in seawater (~2 Ma), as a consequence of its low particle reactivity, impedes the use of radiogenic Sr isotopes as water mass tracer. Nevertheless, the Sr isotope signature of the detrital fraction of the sediment, in particular in combination with Nd isotopes, is a powerful tool for tracing the

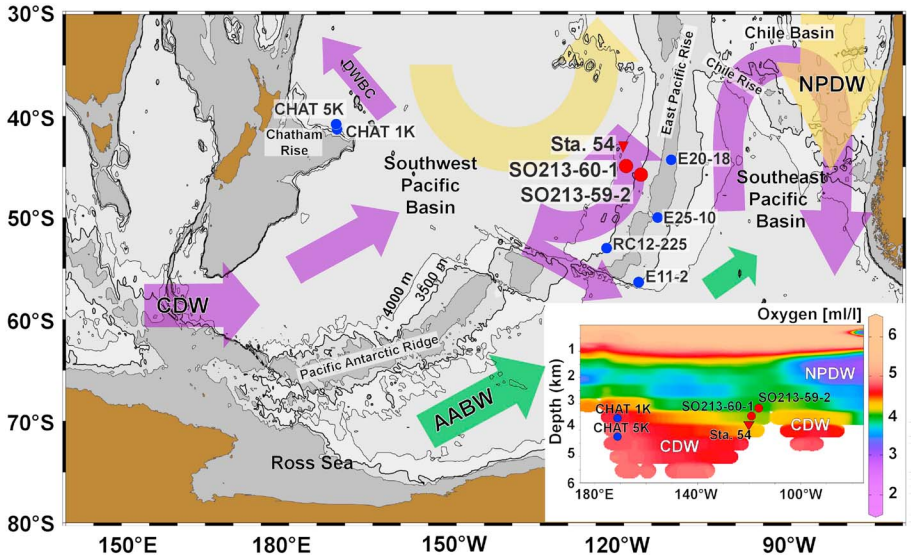

Figure 1. Bathymetric map of the central South Pacific schematically showing flow paths and flow directions of the main water masses between 3000 and 4000 m water depth (circulation patterns after *Reid* [1986] and *Kawabe and Fujio* [2010]). Arrows represent water mass flow coded by colors: Circumpolar Deep Water (CDW) in purple (here comprising both Upper and Lower CDW), Antarctic Bottom Water (AABW) in green, and Pacific-derived waters in yellow, highlighting North Pacific Deep Water (NPDW) to the east of the study area. DWBC = Deep Western Boundary Current. The locations of sediment cores of this study are indicated by red dots: SO213-59-2 (latitude 45°49.736'S, longitude 116°52.761'W, 3161 m water depth), SO213-60-1 (latitude 44°57.831'S, longitude 119°33.071'W, 3471 m water depth). The locations of cores CHAT 1K and CHAT 5K (3556 m and 4240 m water depth, respectively) [*Elderfield et al*., 2012; *Noble et al*., 2013]; E20-18, E25-10, and RC12-225 (2869 m, 2891 m, and 2964 m water depth, respectively) [*Matsumoto and Lynch-Stieglitz*, 1999]; and E11-2 (3094 m water depth) [*Ninnemann and Charles*, 2002] referred to in the text are also included as blue dots. The red triangle marks the water sampling station 54 (latitude 43°S, longitude 120°W, 3842 m water depth) closest to the sediment core locations, where seawater Nd isotope data are available [*Molina-Kescher et al*., 2014a]. On the bottom right corner of the figure, an oxygen section of the area at ~43°S is provided, which represents the structure of the water column and the different water masses, together with the location of some of the studied cores.

climatically driven variability of the provenance of lithogenic material supplied to the Southern Ocean [e.g., *Franzese et al*., 2006; *Noble et al*., 2012].

This study is focused on two sediment cores located on the East Pacific Rise in the central South Pacific. The midlatitude (35°S to 50°S) South Pacific between New Zealand and South America is dominated by a complex deep water circulation pattern, which is schematically shown in Figure 1. The DWBC ($\varepsilon_{Nd} \sim -9.7$) [*Molina-Kescher et al*., 2014a], which detaches from the Antarctic Circumpolar Current (ACC) in the western South Pacific, represents the entrance of deep waters into the Pacific. The exit and reintroduction of old middepth waters (mainly modified North Pacific Deep Water, NPDW, $\varepsilon_{Nd} \sim -5.9$) [*Molina-Kescher et al*., 2014a] flowing from the North Pacific into the ACC occurs in the eastern South Pacific, close to South America (see *Molina-Kescher et al*. [2014a] for a detailed description of the hydrography in the study area). CDW dominates the deep central South Pacific [*Kawabe and Fujio*, 2010], although central Pacific waters also exert some influence at the location of our cores [*Reid*, 1986; *Molina-Kescher et al*., 2014a], which today displays seawater ε_{Nd} signatures of -6.6 [*Molina-Kescher et al*., 2014a]. The Ross Sea is one of the main formation regions of AABW, which occupies the abyssal Southeast Pacific Basin and is characterized by ε_{Nd} signatures near -7 [*Rickli et al*., 2014; *Basak et al*., 2015], but it is not able to cross the East Pacific Rise and the Pacific Antarctic Ridge toward the Southwest Pacific Basin (e.g., the location of our cores) due to its high density [*Orsi et al*., 1999].

In this study, we report evidence based on three independent proxies that have been widely used to track past deep water advection and mixing processes, namely, authigenic, seawater-derived Nd and Pb isotopes, and $\delta^{13}C$ signatures of benthic foraminifera, to reconstruct past changes in central South Pacific deep ocean circulation. Additionally, we show detrital Nd and Sr isotope signatures to infer climatically driven changes in the inputs of detrital material to this region.

2. Samples and Methods

Two gravity cores, SO213-59-2 and SO213-60-1 (from here on referred to as Core 59 and Core 60, respectively), from 3161 m and 3471 m water depth, respectively, obtained on the western flank of the East Pacific Rise in the central South Pacific (44–46°S, 117–119°W) (Figure 1) aboard the German R/V *Sonne* during expedition SO213 (December 2010 to March 2011) [*Tiedemann et al*., 2012] were analyzed for stable oxygen ($\delta^{18}O$) and carbon ($\delta^{13}C$) isotope compositions of benthic foraminifera and for radiogenic neodymium (ε_{Nd}), strontium, and lead isotope compositions of the authigenic and detrital phases of the sediments. The central South Pacific is an area of very low sedimentation rates, which is why we chose not to base our interpretations on the records of one core only.

2.1. Stable Oxygen ($\delta^{18}O$) and Carbon ($\delta^{13}C$) Isotope Analysis

Stable isotope ($\delta^{18}O$ and $\delta^{13}C$) analyses were performed on the benthic foraminiferal species *Cibicidoides wuellerstorfi* for Core 59 ($\delta^{18}O$ data are already published in *Tapia et al*. [2015]) and *Uvigerina peregrina* for Core 60 (~10 individuals of the size fraction >250 μm for both cores). The benthic oxygen isotope variations served to establish the stratigraphy, while $\delta^{13}C$ was intended to be used as a tracer for changes in water mass mixing and to estimate the potential effects of bioturbation on the low sedimentation rate records. Isotopic analyses were performed on a ThermoScientific MAT 253 mass spectrometer coupled with a KIEL IV Carbonate device at AWI and GEOMAR for Core 59 and Core 60, respectively. Results were referenced to the NBS19 standard and calibrated to VPDB. Analytical errors were ±0.03 for both $\delta^{18}O$ and $\delta^{13}C$.

2.2. Nd, Pb, and Sr Isotope Analysis

Seawater Nd and Pb isotope compositions recorded by early diagenetic, authigenic Fe-Mn coatings that precipitate on sediment particles were used to track deep water circulation changes, whereas Nd and Sr isotopes obtained from the continent-derived silicate fraction were used for identifying changes in provenance and inputs of lithogenic material, mainly of dust.

For the extraction of deep water Nd isotope signatures recorded by Fe-Mn coatings we applied the "unclean" planktic foraminifera technique [e.g., *Roberts et al*., 2010; *Tachikawa et al*., 2014] on 63 samples of Core 59 and 40 samples of Core 60. This method has been proven to faithfully reconstruct the Nd isotope composition of deep water in our study area [*Molina-Kescher et al*., 2014b] and other oceanographic regions [e.g., *Roberts et al*., 2010; *Kraft et al*., 2013; *Tachikawa et al*., 2014]. The extraction includes the dissolution of clay-free mixed planktic foraminifera without a preceding separation of Fe-Mn coatings. We also applied a "nondecarbonated" bulk sediment leaching technique, which has proven to be the most reliable leaching method for the isolation of the authigenic Nd from the coatings of bulk sediments [*Wilson et al*., 2013; *Molina-Kescher et al*., 2014b], on 12 samples of each of the two cores to obtain authigenic Pb isotope compositions and to compare the methods for the extraction of seawater-derived Nd isotope compositions. The latter method consists in the leaching of bulk sediment using a 0.05 M hydroxylamine hydrochloride/15% acetic acid solution (HH) buffered to pH 3.6 with NaOH without preceding carbonate removal. In addition, two fish teeth found in Core 60 and one for Core 59 were analyzed to confirm the seawater origin of the extracted Nd isotope compositions, given that this archive has been demonstrated to faithfully record past seawater ε_{Nd} signatures [e.g., *Martin and Scher*, 2004].

Detrital Nd and Sr isotope signatures were obtained on the 24 previously leached bulk sediment samples of Core 59 and Core 60 (plus two more samples for the latter) to track changes in the provenance of the detrital silicates supplied to the core locations. These 26 samples, after a second HH leach of 24 h, were totally digested using a mixture of concentrated HNO_3 and HF. After dissolution all samples underwent a two-step ion chromatographic separation following previously published methods to isolate and purify Nd [*Barrat et al*., 1996; *Le Fevre and Pin*, 2005], Sr [*Horwitz et al*., 1992], and Pb [*Galer and O'Nions*, 1989; *Lugmair and Galer*, 1992].

To measure the isotopic ratios of Nd, Sr, and Pb, we used a Nu Plasma MC-ICPMS at GEOMAR using ratios of 0.7219 for $^{146}Nd/^{144}Nd$ and 0.1194 for $^{88}Sr/^{86}Sr$ to correct for instrumental mass bias. Pb isotope compositions were measured using a standard-sample bracketing method [*Albarède et al*., 2004]. Nd and Sr isotope ratios were corrected for ^{144}Sm and ^{86}Kr, ^{87}Rb interferences, respectively. All results were normalized to the accepted values of 0.512115 (JNdi-1 standard [*Tanaka et al*., 2000]) for $^{143}Nd/^{144}Nd$, 0.710245 (NIST

AGU Paleoceanography

10.1002/2015PA002863

Table 1. Results of This Study Averaged for Isotopic Stages[a]

S0213-59-2	$\delta^{18}O$	2σ	n	SD	$\delta^{13}C$ Benthic	2σ	n	SD	ε_{Nd} Forams	2σ	n	SD	ε_{Nd} Leachates	2σ	n	SD	ε_{Nd} Detritus	2σ	n	SD
Holocene	3.15	±0.06	9	0.24	0.34	±0.07	9	0.18	−5.78	±0.25	5	0.29	−5.95	±0.40	1	-	−5.24	±0.24	1	
MIS 2	4.21	±0.06	22	0.17	−0.05	±0.07	22	0.10	−5.22	±0.25	6	0.54	−5.33	±0.40	1	-	−3.76	±0.24	1	-
Last Interglacial (MIS 3 + 4 + 5)	3.79	±0.06	78	0.28	0.28	0.28	78	0.19	−5.80	±0.25	26	0.20	−5.52	±0.40	5	0.18	−4.70	±0.24	5	0.51
MIS 6	4.19	±0.06	16	0.20	−0.36	±0.07	16	0.18	−5.29	±0.25	11	0.18	−4.06	±0.40	2	0.09	−4.28	±0.24	2	0.18
MIS 7	3.90	±0.06	21	0.40	−0.20	±0.07	21	0.32	−5.69	±0.25	15	0.32	−4.96	±0.40	3	0.57	−5.34	±0.24	3	0.37
Average Interglacials[b]	3.75	±0.06	108	0.35	0.08	±0.07	108	0.27	−5.76	±0.25	46	0.26	−5.37	±0.40	8	0.50	−5.08	±0.24	8	0.44
Average glacials	4.20	±0.06	38	0.18	−0.18	±0.07	38	0.21	−5.26	±0.25	17	0.33	−4.73	±0.40	4	0.78	−4.11	±0.24	4	0.27

	$^{206}Pb/^{204}Pb$ Leach	2σ	n	SD	$^{207}Pb/^{206}Pb$ Leach	2σ	n	SD	$^{208}Pb/^{204}Pb$ Leach	2σ	n	SD	$^{87}Sr/^{88}Sr$ Detritus	2σ	n	SD
Holocene	18.771	±0.015	1	-	0.8324	±0.0001	1	-	38.68	±0.015	1	-	0.70925	0.00004	1	-
MIS 2	18.738	±0.015	1	-	0.8333	±0.0001	1	-	38.60	±0.015	1	-	0.70933	0.00004	1	-
Last Interglacial (MIS 3 + 4 + 5)	18.758	±0.015	5	0.009	0.8327	±0.0001	5	0.0006	38.63	±0.015	5	0.03	0.70935	0.00004	5	0.00009
MIS 6	18.747	±0.015	2	0.008	0.8334	±0.0001	2	0.0004	38.63	±0.015	2	0	0.70935	0.00004	2	0.00001
MIS 7	18.755	±0.015	2	0.006	0.8331	±0.0001	2	0.0002	38.64	±0.015	2	0	0.70937	0.00004	3	0.00012
Average Interglacials[b]	18.759	±0.015	8	0.009	0.8327	±0.0001	8	0.0005	38.64	±0.015	8	0.02	0.70935	0.00004	9	0.00010
Average glacials	18.744	±0.015	3	0.008	0.8333	±0.0001	3	0.0003	38.62	±0.015	3	0.02	0.70934	0.00004	3	0.00002

S0213-60-1	$\delta^{18}O$ Benthic	2σ	n	SD	$\delta^{13}C$ Benthic	2σ	n	SD	ε_{Nd} Forams	2σ	n	SD	εNd Leachates	2σ	n	SD	εNd Detritus	2σ	n	SD
Holocene	3.07	±0.06	1	-	−0.22	±0.07	1	-	−5.91	±0.32	2	0.17	−6.02	±0.40	1	-	−5.24	±0.24	1	-
MIS 2	4.27	±0.06	4	0.17	−0.50	±0.07	4	0.17	−5.76	±0.32	4	0.36	-	±0.40	-	-	−4.07	±0.24	1	-
Last Interglacial (MIS 3 + 4 + 5)	4.21	±0.06	37	0.25	−0.42	±0.07	37	0.17	−5.80	±0.32	19	0.24	−5.85	±0.40	7	0.35	−5.53	±0.24	7	0.25
MIS 6	4.43	±0.06	19	0.22	−0.89	±0.07	19	0.14	−5.53	±0.32	10	0.46	−6.05	±0.40	2	0.48	−5.38	±0.24	3	0.51
MIS 7	4.03	±0.06	10	0.26	−0.73	±0.07	10	0.23	−5.86	±0.32	4	0.31	−5.85	±0.40	2	0.20	−5.82	±0.24	2	0.22
Average Interglacial[b]	4.15	±0.06	48	0.30	−0.48	±0.07	48	0.23	−5.82	±0.32	25	0.24	−5.87	±0.40	10	0.30	−5.56	±0.24	10	0.27
Average glacials	4.40	±0.06	23	0.22	−0.83	±0.07	23	0.19	−5.60	±0.32	14	0.43	−6.05	±0.40	2	0.48	−5.05	±0.24	4	0.78

	$^{206}Pb/^{204}Pb$ Leach	2σ	n	SD	$^{207}Pb/^{206}Pb$ Leach	2σ	n	SD	$^{208}Pb/^{204}Pb$ Leach	2σ	n	SD	$^{87}Sr/^{88}Sr$ Detritus	2σ	n	SD
Holocene	18.751	±0.015	1	-	0.8331	±0.0001	1	-	38.66	±0.015	1	-	0.70934	0.00004	1	-
MIS 2	-	±0.015	1	-	-	±0.0001	1	-	-	±0.015	1	-	0.71023	0.00012	1	-
Last Interglacial (MIS 3 + 4 + 5)	18.760	±0.015	7	0	0.8328	±0.0001	7	0.0003	38.66	±0.015	7	0.02	0.70938	0.00004	7	0.00014
MIS 6	18.758	±0.015	3	0.005	0.8333	±0.0001	3	0.0002	38.67	±0.015	3	0.01	0.70955	0.00004	3	0.00030
MIS 7	18.775	±0.015	2	0.006	0.8327	±0.0001	2	0.0001	38.70	±0.015	2	0.01	0.70929	0.00008	2	0.00006
Average Interglacials[b]	18.762	±0.015	10	0.009	0.8328	±0.0001	10	0.009	38.67	±0.015	10	0.02	0.70936	0.00004	10	0.00013
Average glacials	18.758	±0.015	4	0.004	0.8333	±0.0001	4	0.0002	38.67	±0.015	4	0.04	0.70972	0.00010	4	0.00042

[a]The averages for each stage were calculated using all available data points for each period (n) (see data in Tables S1 and S2). "SD" stands for standard deviation of "n."
[b]Including here glacial MIS 4.

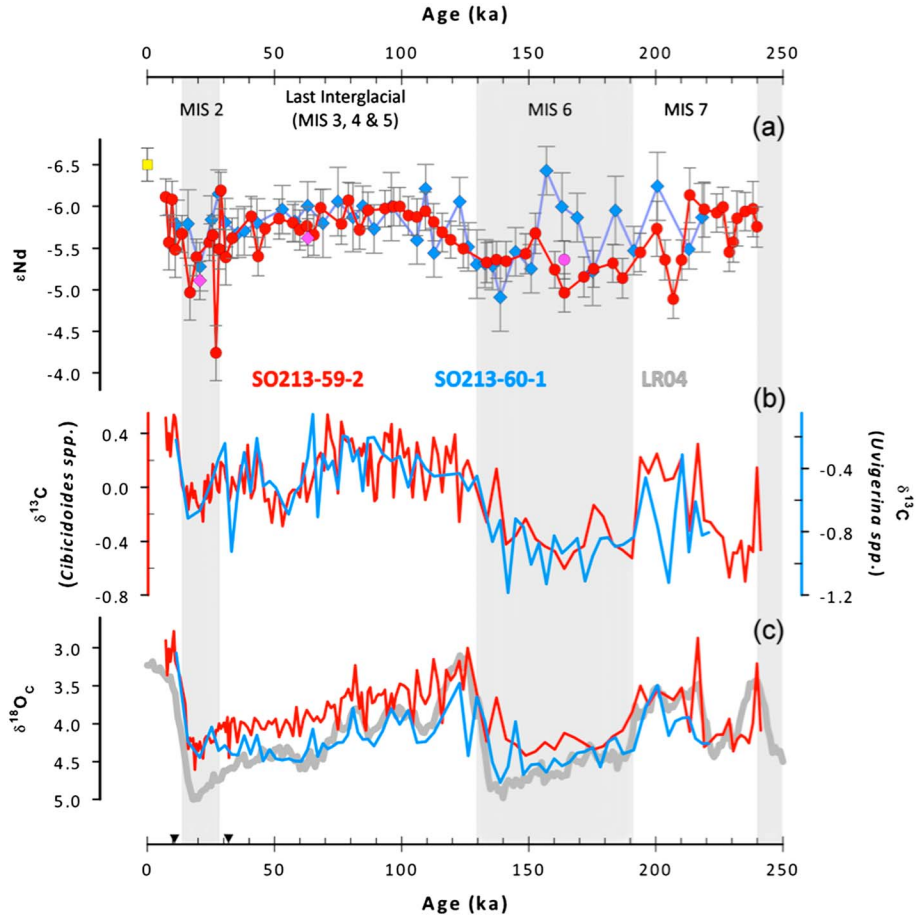

Figure 2. (a) Nd isotope data (ε_{Nd} with 2σ error bars) of Core SO213-59-2 (red circles) and SO213-60-1 (blue diamonds) for the past ~240 ka B.P. The ε_{Nd} data reflect the isotopic composition of seawater during the studied period of time obtained from Fe-Mn coatings of unclean planktic foraminifera and fish teeth (pink dots). Present-day seawater ε_{Nd} from station 54 (see Figure 1) is represented by a yellow square at 0 ka B.P. [*Molina-Kescher et al.*, 2014a]. In comparison, (b) carbon ($\delta^{13}C$) and (c) oxygen ($\delta^{18}O$) isotopes obtained from the benthic foraminifera *Cibicidoides wuellerstorfi* (SO213-59-2, red) and *Uvigerina peregrina* (SO213-60-1, blue) are shown. The age models of cores SO213-59-2 [*Tapia et al.*, 2015] and SO213-60-1 are based on the visual correlation of the benthic $\delta^{18}O$ record to the global $\delta^{18}O$ reference stack LR04 (grey line) [*Lisiecki and Raymo*, 2005], in the case of SO213-59-2 supported by AMS ^{14}C datings (black triangles). Shaded areas define full glacial marine isotope stages (MIS).

NBS987) for $^{87}Sr/^{86}Sr$, and to the accepted values of NBS981 [*Abouchami et al.*, 1999] for Pb isotopes. The external reproducibilities (2σ) of the Nd, Sr, and Pb isotope measurements during each session were assessed by repeated measurements of the above standards matching sample concentrations and ranged between 0.2 and 0.4 ε_{Nd} units, between 0.00004 and 0.00012 for $^{87}Sr/^{86}Sr$, and 0.015 for $^{206}Pb/^{204}Pb$, 0.0001 for $^{207}Pb/^{206}Pb$, and 0.015 for $^{208}Pb/^{204}Pb$ (see Table 1).

2.3. Stratigraphy

The age models of Cores SO213-59-2 and SO213-60-1 are based on $\delta^{18}O$ records of the benthic foraminifera species *Cibicidoides wuellerstorfi* and *Uvigerina peregrina*, respectively, tuned to the global benthic $\delta^{18}O$ stack LR04 [*Lisiecki and Raymo*, 2005] for the past ~240,000 years (Core 59) and ~221,000 years (Core 60) (Figure 2c). The age model of Core 59 [*Tapia et al.*, 2015] is supported by two ^{14}C accelerator mass spectrometer (AMS) ages at 10.7 ± 0.1 and 33.5 ± 0.4 kiloyears before present, further on referred to as ka B.P. The sediments of this core were deposited at low sedimentation rates between 0.4 cm ka^{-1} B.P. and 1.5 cm ka^{-1} B.P. but nevertheless allow a clear differentiation of the most prominent orbitally forced climatic transitions of the last two glacial cycles. The glacial marine isotope stages (defined after *Lisiecki and Raymo* [2005]) MIS 6 (191–130 ka B.P.) and 2 (29–14 ka B.P.) yield an average benthic $\delta^{18}O$ value of 4.2‰, identical to average global and South

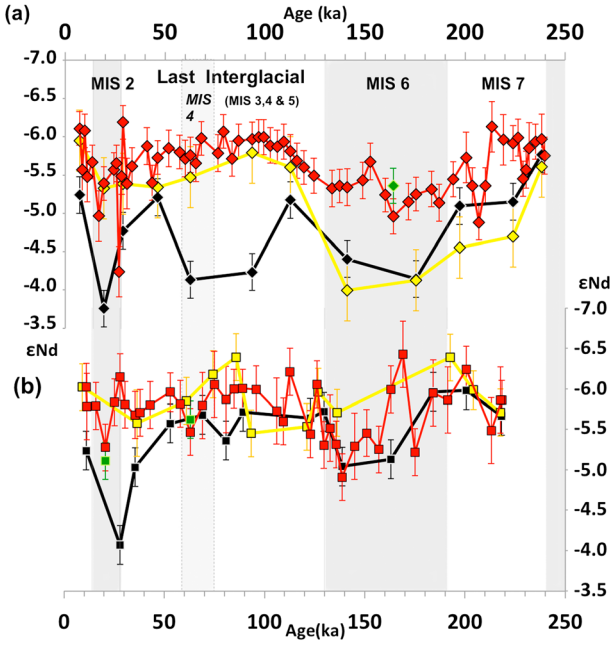

Figure 3. Comparison of Nd isotope compositions (ε_{Nd}) obtained from different fractions of the sediment (authigenic and detrital) and using different techniques (unclean forams, leachates, and fish teeth) in order to elucidate the reliability of the seawater-derived signal (see section 4.1) for cores (a) SO213-59-2 in diamonds and (b) SO213-60-1 in squares for the last 240 and 220 ka B.P., respectively. ε_{Nd} signatures are given in black for the detrital fraction of the sediment, the nondecarbonated leachates in yellow, the unclean forams in red, and the fish teeth in green. Shaded areas define full glacial marine isotope stages (MIS).

Pacific Last Glacial Maximum (LGM) values for the same species [*Matsumoto and Lynch-Stieglitz*, 1999]. The $\delta^{18}O$ difference between available Holocene samples (7–14 ka B.P.) and the maxima of the glacial periods MIS 2 and MIS 6 is 1.1‰, close to the expected global ice volume change of 1.2‰ [*Elderfield et al.*, 2012]. The last interglacial (29–130 ka B.P.), here represented by MIS 3 to MIS 5 (including short glacial MIS 4, which cannot be clearly distinguished in our record), displays a progressive transition from minimum $\delta^{18}O$ values of ~3‰ at MIS 5e (~126 ka B.P.) to maximum values of ~4.6‰ recorded for the LGM.

Despite the fact that the age model of second Core 60 lacks ^{14}C datings, the stratigraphy is well constrained by the benthic $\delta^{18}O$ curve and fully supported by biostratigraphic and paleomagnetic data. Core 60 presents lower sedimentation rates (0.4 cm ka B.P.$^{-1}$ to 1.0 cm ka B.P.$^{-1}$) than Core 59, but the benthic oxygen isotope data show the expected glacial-interglacial amplitudes in both cores (Figure 2c), therefore discarding significant bioturbation effects on the records. The offset observed between the two $\delta^{18}O$ records is most probably due to a vital effect between the two species, given that *Cibicidoides wuellerstorfi* lives epifaunally, whereas *Uvigerina peregrina* is a shallow infaunal species [*Gooday*, 2003]. The Holocene is only covered by one sample for this core at 11 ka.

3. Results

3.1. Authigenic Nd Isotopes

Deep water Nd isotope compositions obtained from unclean foraminifera of Cores 59 and 60, which are at present bathed in CDW, yield within error the same average ε_{Nd} signatures of −5.6 and −5.7, respectively. Both cores recorded only relatively small variations during the entire investigated period of time (Figure 2a), which reflects the mixing proportions of the different water masses contributing to CDW. In general, less radiogenic ε_{Nd} signatures prevailed during interglacial periods, which average −5.8 in both cores and show minimum ε_{Nd} values of −6.1. In contrast, the most radiogenic ε_{Nd} signatures occurred during glacials with averages of −5.3 for Core 59 and −5.6 for Core 60, with maximum ε_{Nd} values of up to −4.2. The consistent difference between the glacial and interglacial ε_{Nd} averages (Table 1) is small for both cores, but it is systematic and significant, at least in the case of higher resolved Core 59. The data of Core 60 generally follow the same trend as Core 59 including a radiogenic peak near the LGM and a clear transition from more radiogenic, "Pacific-like" (−4.9) to less radiogenic "Southern Ocean-like" (−6.1) ε_{Nd} values at the MIS 6 to MIS 5 transition. Only in the interval between 159 and 181 ka B.P. in Core 60, two samples clearly deviate toward less radiogenic values (−6 and −6.4 ε_{Nd} units) and thus do not match the general trend displayed by Core 59 (Figure 2a). A fish tooth Nd isotope signature from a section with an age of 164 ka B.P. in Core 59 confirms the overall more positive glacial ε_{Nd} signatures obtained from the unclean foraminifera of MIS 6. The two fish teeth found in Core 59 at 20.6 ka B.P. (ε_{Nd} −5.1) and 63.1 ka B.P. (ε_{Nd} −5.6) match the corresponding unclean foraminifera data within error.

The ε_{Nd} signatures of the nondecarbonated leachates of Core 59 (Figure 3a) are within error identical to those of the unclean foraminifera in the younger part of the core between MIS 5 and the present. For

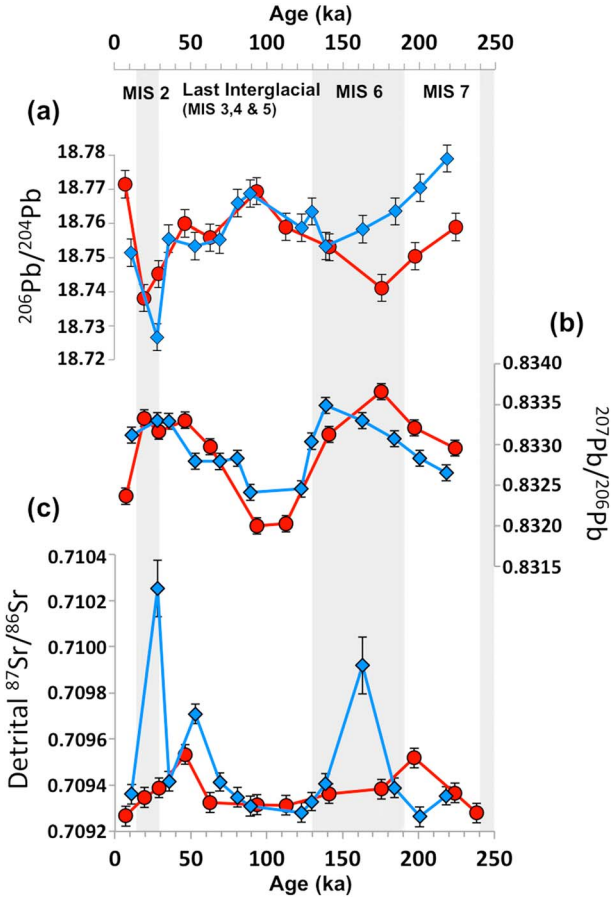

Figure 4. Authigenic Pb isotope compositions of nondecarbonated bulk sediment leachates and detrital Sr isotope compositions for cores SO213-59-2 (red circles) and SO213-60-1 (blue diamonds) for the last ~240 and ~220 ka B.P., respectively. (a) $^{206}Pb/^{204}Pb$ ratios, (b) $^{207}Pb/^{206}Pb$ ratios, and (c) $^{87}Sr/^{86}Sr$ 2σ error bars are indicated. Shaded areas define full glacial marine isotope stages (MIS).

MIS 6 and most of MIS 7 the leachate data are significantly more radiogenic and closely match the detrital data, suggesting contamination with the latter fraction of the sediment (see section 4.1). Leachate Nd isotope signatures of Core 60 (Figure 3b) are identical within error to the detrital and unclean foraminifera data for most samples, and there are no systematic offsets between the two methods for extraction of the seawater signatures.

3.2. Authigenic Pb Isotopes

$^{206}Pb/^{204}Pb$ and $^{207}Pb/^{206}Pb$ leachate results of both cores chosen for display in Figure 4 (see also Table 1 and supporting information Tables S1 and S2) show values similar to Fe-Mn nodules obtained from the central South Pacific at similar latitudes [*Abouchami and Goldstein*, 1995]. The glacial-interglacial variations in the Pb isotope ratios in both records are relatively small but clearly significant. They are consistent between the two locations and of essentially the same amplitude of glacial to interglacial change (Figure 4). The variability follows the same pattern as the seawater-derived ε_{Nd} signatures and the benthic $\delta^{13}C$ values in that more Pacific-like signatures prevailed during glacial stages, suggesting a common factor controlling the changes of the three different deep water circulation proxies (see section 4.2).

3.3. Benthic Carbon Isotopes

The variations in the benthic $\delta^{13}C$ signature of Core 59 recorded by *Cibicidoides wuellerstorfi* follow trends very similar to those of benthic $\delta^{18}O$ of the same record (Figure 2). The LGM (19–23 ka) to Holocene (youngest available data: 7–8 ka) difference in $\delta^{13}C$ reaches 0.51‰, which is 0.12‰ larger than recent estimates of terrestrial carbon reservoir changes for the South Pacific of 0.39‰ [*Peterson et al*., 2014]. Glacial stages MIS 2 and MIS 6 display markedly different average $\delta^{13}C$ values (−0.05 and −0.36, respectively), which differ considerably between each other, with a sharp drop of about 0.7‰ observed for the MIS 7 to MIS 6 transition. These values are similar to those of other studies from the Southern Hemisphere [*Oliver et al*., 2010; *Peterson et al*., 2014], in general, and from the central South Pacific [*Matsumoto and Lynch-Stieglitz*, 1999; *Ninnemann and Charles*, 2002] in particular (Figure 5), supporting the absence of significant effects of bioturbation on the record of our core. Benthic $\delta^{13}C$ signatures of Core 60 (Figure 2b), obtained from infaunal species *Uvigerina peregrina*, display slightly less pronounced changes though with similar amplitude and overall lighter carbon isotope compositions than Core 59 as a consequence of growth from isotopically light pore waters due to respiration processes [*Ravelo and Hillaire-Marcel*, 2007].

3.4. Detrital Provenance Proxies (Nd and Sr Isotopes)

Nd and Sr isotopes obtained from the detrital fraction of the sediment serve to trace provenance of continental-derived silicates arriving in the central South Pacific during the studied interval of time. Except for one sample of the last interglacial at 93.5 ka B.P. (MIS 5c), the detrital ε_{Nd} signatures of Core 59 (black

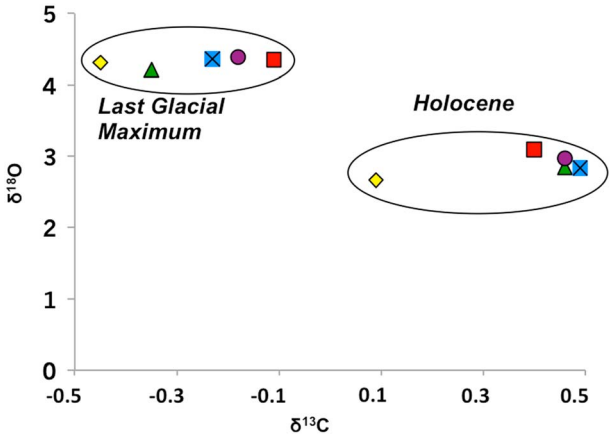

Figure 5. Comparison of average stable oxygen ($\delta^{18}O$) versus carbon ($\delta^{13}C$) isotope compositions of benthic foraminifera (*Cibicidoides*) for all available central South Pacific cores (see locations of Figure 1) for the Last Glacial Maximum and the Holocene. Red squares: Core SO213-59-2 (this study), yellow diamonds: E11-2 [*Ninnemann and Charles*, 2002], green triangles: E20-18, blue crosses: E25-10, and purple circles: RC12-225 [*Matsumoto and Lynch-Stieglitz*, 1999].

diamonds on Figure 3a) show glacial-interglacial variations oscillating between more radiogenic glacial signatures (−3.5 to −4.5) and less radiogenic interglacial signatures (−5 to −6) suggesting systematic changes in the provenance of the lithogenic material that reached the study area during cold and warm periods (see section 4.3). A higher proportion of mantle-like source rocks prevailed during glacial periods. Except for a radiogenic peak value near −4 at the LGM, the glacial/interglacial differences in the detrital ε_{Nd} data of Core 60 are less pronounced than for Core 59, ranging between ~−5 and ~−6 (black squares in Figure 3b).

Detrital Sr isotope ratios ($^{87}Sr/^{86}Sr$) show a small range between 0.7092 and 0.7095 for Core 59 and between 0.7092 and 0.7102 for Core 60 (Figure 4c). While Core 59 does not reveal systematic glacial-interglacial detrital $^{87}Sr/^{86}Sr$ variations, Core 60 shows peaks of radiogenic values during glacials indicating a lower proportion of mantle-derived source rocks.

4. Discussion

4.1. Reliability of the Nd and Pb Isotope Data as Recorder of Past Deep Water Circulation

Before we interpret the extracted deep water Nd isotope signatures, their reliability needs to be evaluated. Fossil fish teeth are known to faithfully record the Nd isotope composition of bottom waters of the past [*Martin and Scher*, 2004]. The three fossil fish teeth measured in this study display within error the same ε_{Nd} signatures as unclean foram fractions of the same samples (Figures 2 and 3 and Tables S1 and S2). Comparison to the Nd isotope compositions of the detritus (Figure 3) supports the absence of any significant contamination of the seawater signal extracted from the foraminifera in agreement with the results obtained for the surface sediments [*Molina-Kescher et al.*, 2014b]. In particular, the detrital ε_{Nd} signatures of Core 59 (Figure 3a) in most cases show considerably more radiogenic ε_{Nd} values than the unclean foram fraction, which is most pronounced during glacial periods, when the detritus reached the most positive values and the difference to the unclean foram data amounted to up to 1.6 ε_{Nd} units. In core 60-2 (Figure 3b), most of the detrital and unclean foram Nd isotope compositions are similar.

In addition to the above considerations, both cores recorded consistent LGM (~21 ka B.P.) to early Holocene trends from more radiogenic (5.0 ± 0.3 and −5.3 ± 0.3 for Cores 59 and 60, respectively) to less radiogenic ε_{Nd} signatures (−6.1 ± 0.3 at 7.1 ka B.P. for Core 59 and −6.0 ± 0.3 at 11.3 ka B.P. for Core 60) of the unclean foraminifera (Figure 2a). These youngest samples available for our cores agree within error with present-day seawater signatures at the same location [*Molina-Kescher et al.*, 2014a], which displays a value of −6.5 ± 0.2 at 3842 m water depth (see Figure 2a). An essentially identical trend is observed for the transition from MIS 6 to MIS 5 on both cores. Although generally low sedimentation rates of 0.5–2 cm ka B.P.$^{-1}$ prevail in the study area [*Tiedemann et al.*, 2012], any influence of bioturbation on the amplitudes of the changes in Nd isotope signatures is considered negligible given that the benthic oxygen and carbon isotope data (see section 4.2.2.) show the expected glacial-interglacial amplitudes in both cores.

The nondecarbonated leachates did apparently not always record the seawater signal as reliably as the unclean forams. This is most evident in Core 59 (Figure 3a), where leachates faithfully follow the seawater curve of the foraminifera back to 130 ka B.P., whereas prior to that, the similarity between the detrital and leachate signatures suggests a possible contamination of the latter by partial dissolution of the lithogenic fraction during the leaching process. Certainly, this issue does not affect the unclean foraminifera data as confirmed by the fish tooth found at 164 ka B.P. in Core 59 (ε_{Nd} −5.4), which matches the foraminifera data.

Contributions from sedimentary pore waters [*Haley et al*., 2004; *Abbot et al*., 2015a, 2015b] may have affected the nondecarbonated leach signal of the older part of Core 59, despite that this core was retrieved on a low sedimentation rate area not prone to develop anoxic conditions in subsurface sediments and to the release of significant sedimentary REE fluxes. Further evidence for the absence of a significant pore water influence on the unclean foraminifera ε_{Nd} data on this area comes from the typical seawater pattern of normalized Post-Archean Australian Sedimentary Rock (PAAS) REEs observed on core tops (see discussion in *Molina-Kescher et al*. [2014b]). Leachates of Core 60 (Figure 3b) show ε_{Nd} values similar to those of the forams and the detritus. Given the differences observed in Core 59, we will only use the unclean foraminifera data of both cores for the paleoceanographic interpretations of this study, which have been documented to reliably record past deep water signatures in the South Pacific and other areas [*Roberts et al*., 2010; *Kraft et al*., 2013; *Tachikawa et al*., 2014; *Molina-Kescher et al*., 2014b]

The Pb isotope data were obtained using the nondecarbonated leach technique, but the absence of detrital Pb isotope data does not allow the evaluation of a possible detrital contamination from pore waters. However, the very high particle reactivity of Pb makes any mobilization from pore waters highly unlikely and the leaching method has been shown to yield reliable seawater Pb isotope data [*Gutjahr et al*., 2009; *Stumpf et al*., 2010; *Crocket et al*., 2012; *Wilson et al*., 2015b; *Teschner et al*., 2016] and the consistent glacial-interglacial variations, as well as the close agreement of our Pb isotope results with the ferromanganese crust data of *Abouchami and Goldstein* [1995] for the same region support the validity of our results.

4.2. Changes in the Deep Water Circulation of the Last Two Glacial Cycles

Nd, Pb, and C isotopes of Core 59 (Figures 2 and 4) generally show consistent glacial-interglacial variations indicating more Pacific-like signatures during glacial periods. Paleoceanographic changes in the South Pacific Ocean have been poorly studied compared to other oceanic regions, but there is evidence for a deepening of NPDW during the last glacial period [*Keigwin*, 1998; *Matsumoto and Lynch-Stieglitz*, 1999; *Matsumoto et al*., 2002; *Huang et al*., 2014]. Although these changes may partly explain the glacial-interglacial variations observed in our data, the flow of NPDW from the Pacific into the Southern Ocean today principally occurs at middepths of the eastern South Pacific [e.g., *Kawabe and Fujio*, 2010; *Molina-Kescher et al*., 2014a], whereas the central South Pacific is not an exit of Pacific deep waters to the ACC. Rather, this area represents a main entrance area of UCDW flowing into the Pacific, although at shallower depths than the location of our cores [see *Kawabe and Fujio*, 2010]. Therefore, it is unlikely that a deepening or stronger production of NPDW during glacial stages fully explains the long-term deep water circulation changes observed in the central South Pacific. Instead, these processes would be better recognizable in the eastern South Pacific, where a more vigorous glacial advection of NPDW may have occupied parts of the SE Pacific Basin during the last glacial period that are today dominated by Circumpolar Deep Water [*Molina-Kescher et al*., 2014b].

Given the position of our cores (44°–46°S), the bathymetry of the South Pacific, and the eastward flow of the ACC (see circulation scheme in Figure 1), it is also very unlikely that dense AABW formed in the Ross Sea (Ross Sea Deep Water) and characterized by $\varepsilon_{Nd} = \sim -7.0$ [*Rickli et al*., 2014; *Basak et al*., 2015], reached the western flank of the E Pacific Rise at the water depth of our cores in the past. Our data do also not support a hypothetical admixture of AABW formed in the Weddell Sea during glacials as this water mass is characterized by significantly less radiogenic ε_{Nd} signatures (-9.5) [*van de Flierdt et al*., 2007; *Stichel et al*., 2012a].

In contrast, there is compelling paleoceanographic evidence deduced from both carbon [e.g., *Boyle and Keigwin*, 1986; *Duplessy et al*., 1988; *Charles and Fairbanks*, 1992; *Ninnemann and Charles*, 2002; *Curry and Oppo*, 2005; *Gebbie*, 2014] and Nd isotopes [*Rutberg et al*., 2000; *Piotrowski et al*., 2004, 2005, 2008, 2009, 2012; *Noble et al*., 2013] indicating reduced NADW export to the Southern Ocean during cold climate stages of the past. Combination with Pa/Th ratios [e.g., *McManus et al*., 2004; *Roberts et al*., 2010; *Böhm et al*., 2015] showed a shoaling of NADW [*Curry and Oppo*, 2005; *Adkins*, 2013; *Ferrari et al*., 2014; *Böhm et al*., 2015; *Wilson et al*., 2015a] and a reduced NADW production [*Piotrowski et al*., 2005; *Robinson and van de Flierdt*, 2009; *Pena and Goldstein*, 2014]. Hence, the diminished contribution of NADW to CDW during cold stages is the most probable explanation for the variations observed in our Nd and the Pb isotope data.

4.2.1. Nd and Pb Isotope Evidence of Decreased Admixture of NADW to CDW

At the present day, the western flank of the East Pacific Rise at the depth of our core locations between 3000 and 3500 m is mainly bathed in CDW (see Figure 1). Nevertheless, the present-day hydrographic properties also indicate a significant influence of Pacific-derived waters at this location and depth as reflected by

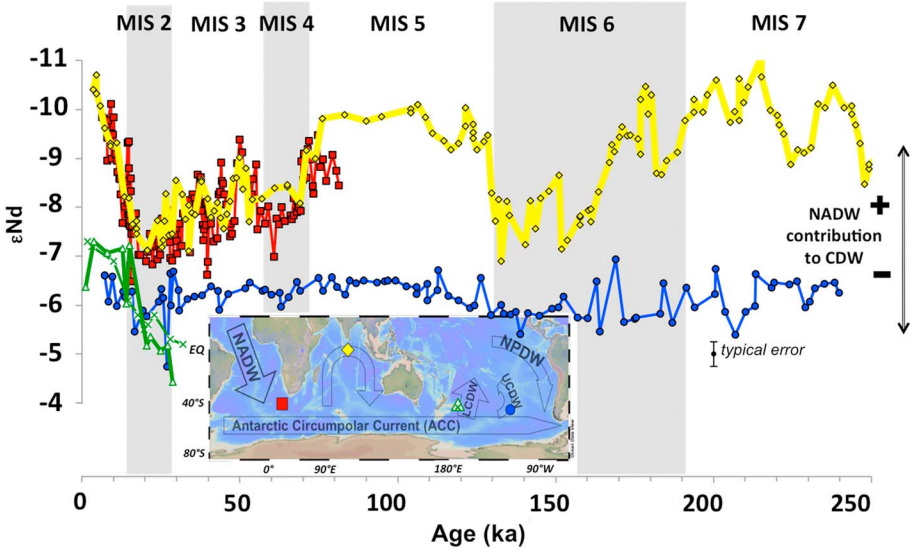

Figure 6. Comparison of Southern Hemisphere Nd isotope (ε_{Nd}) records from comparable water depths but different oceanic settings (see inset map) covering similar time scales. Increasing ε_{Nd} (note reverse scale) implies gradually diminishing influence of NADW toward east. Red squares: cores RC11-83/TNO57-21 from 4718/4981 m water depth [*Piotrowski et al.*, 2005, 2008]; yellow diamonds: core SK129-CR2 from 3800 m water depth [*Piotrowski et al.*, 2009; *Wilson et al.*, 2015a]; green triangles and crosses: cores CHAT 1K [*Elderfield et al.*, 2012] and CHAT 5K [*Noble et al.*, 2013] from 3556 m and 4240 m water depth, respectively; and blue circles: core SO213-59-2 from 3161 m water depth (this study). Shaded areas define full glacial marine isotope stages (MIS).

relatively radiogenic Nd isotope compositions (−6.5) as well as decreased oxygen levels (~3.8 mL/L) and elevated phosphate concentrations (2.16 mmol/L) [*Molina-Kescher et al.*, 2014a]. For comparison, pure Lower CDW (LCDW) in the Southwest Pacific Basin is characterized by $\varepsilon_{Nd} = -8.3$, $[O_2] = 4.4$ mL/L and [Phosphate] = 2.07 mmol/L [*Molina-Kescher et al.*, 2014a]. Therefore, the admixture of Pacific central waters to the deep waters of the study area further dilutes the fraction of NADW present in CDW, which contributes to the relatively small glacial-interglacial Nd isotope variations. This dilution effect with Pacific central waters is also evident when comparing our ε_{Nd} record of Core 59 to Holocene and LGM Nd isotope compositions obtained at CHAT 5K and CHAT 1K (Figure 6) on Chatham Rise in the western South Pacific from a water depth of 3290 m [*Elderfield et al.*, 2012; *Noble et al.*, 2013], which is located in the main entrance area of CDW into the Pacific Basin and consequently still contains a higher proportion of NADW compared to the central South Pacific [*Reid and Lynn*, 1971; *Warren*, 1973; *Gordon*, 1975; *McCave et al.*, 2008]. The LGM to Holocene amplitude of the change of Cores CHAT 1K and CHAT 5K (~2 ε_{Nd} units) is significantly larger than that observed for Core 59 (1 to 1.5 ε_{Nd} units) consistently reflecting the higher proportion of unradiogenic NADW within CDW for Sites CHAT 1K and CHAT 5K.

The presence of NADW on deep waters of the Southern Hemisphere decreases along the flow path of the deep THC toward the east, reflecting the progressive dilution of NADW as it mixes with other water masses. This is reflected by the overall progressively more radiogenic ε_{Nd} signatures and the decrease of the glacial/interglacial Nd isotope differences (Figure 6) from the South Atlantic (red squares: Core RC11-83/TNO57-21) [*Piotrowski et al.*, 2008] and the Indian Ocean (yellow diamonds: Core SK129-CR2) [*Piotrowski et al.*, 2009; *Wilson et al.*, 2015a] via the western South Pacific (Green triangles: Cores CHAT 1K and CHAT 5K) [*Elderfield et al.*, 2012; *Noble et al.*, 2013] to the central South Pacific (Blue circles: Core 59, this study). Although a change in the preformed Nd isotope composition of NADW through time cannot be completely excluded [*Gutjahr et al.*, 2008; *Wilson et al.*, 2014], we here assume no change on glacial-interglacial time scales based on evidence inferred from Fe-Mn crust and deep water coral data from the western North Atlantic [*Foster and Vance*, 2006; *van de Flierdt et al.*, 2006]. Therefore, either a reduction in the production rate and admixture of NADW [e.g., *Piotrowski et al.*, 2005; *Robinson and van de Flierdt*, 2009; *Pena and Goldstein*, 2014], a shoaling of the latter [e.g., *Wilson et al.*, 2015a; *Adkins*, 2013], or a combination of both processes during cold stages is the most probable explanation for the ε_{Nd} variations observed in the Southern Ocean locations presented in Figure 6.

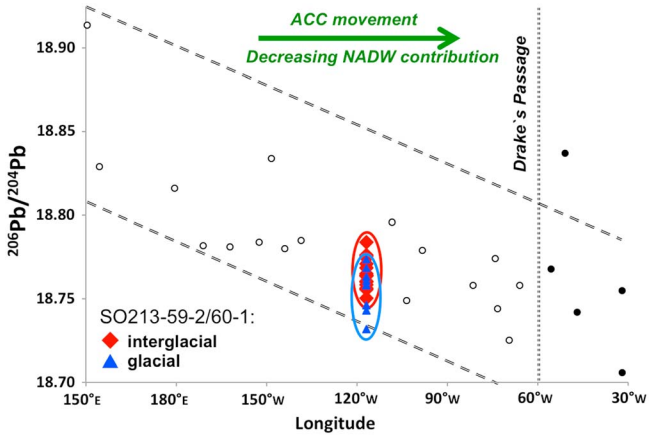

Figure 7. $^{206}Pb/^{204}Pb$ evolution of CDW along the ACC pathway as a consequence of decreased NADW contribution and comparison with glacial/interglacial signatures of the central South Pacific of this study. $^{206}Pb/^{204}Pb$ versus longitude along the ACC showing Pb isotope compositions of Fe-Mn nodules of the South Pacific (open circles) and the southwest Atlantic (black circles) (data from *Abouchami and Goldstein* [1995]) in comparison with Fe-Mn leachates of cores SO213-59-2 and SO213-60-1 (this study). The latter are separated into interglacial (red diamonds) and glacial (blue triangles) isotope ratios. Dashed lines indicate the change in the range of Pb isotope compositions of CDW with longitude. Figure modified from *Abouchami and Goldstein* [1995].

The small but significant variations found in the $^{206}Pb/^{204}Pb$ and $^{207}Pb/^{206}Pb$ records (Figures 3a and 3b) also confirm the lowered portion of North Atlantic sourced deep waters within CDW of the South Pacific. *Abouchami and Goldstein* [1995] presented a detailed study of the evolution of Pb isotope signatures along the pathway of Circumpolar Deep Water in the ACC (see Figure 7). Despite the short residence time of Pb in seawater, a continuous decrease of the $^{206}Pb/^{204}Pb$ ratio toward the east (East Atlantic/Indian > Pacific > West Atlantic) within CDW reflects the dilution of NADW along the pathway of CDW, with maximum values of 19.10 in the southern Indian Ocean and minimum values of 18.70 in the eastern South Pacific and western South Atlantic. The cores systematically show minimum values of ~18.73 for MIS 2 and the beginning of MIS 6 and maxima of ~18.78 during the Holocene, MIS 5, and MIS 7 (Figure 7), in agreement with the changes in NADW admixture to CDW deduced from the Nd isotope signatures above.

4.2.2. Influence of Terrestrial Carbon Reservoir Changes in the $\delta^{13}C$ Record

As recently demonstrated by the compilation of *Peterson et al*. [2014], the LGM-Holocene variation in $\delta^{13}C$ signatures due to changes in the proportion of the global carbon reservoirs between the land and the ocean reaches 0.39‰ for deep waters of the South Pacific region. In the case of Core 59, this difference amounts to 0.51‰, which includes the latter 0.39‰ variation and leaves a 0.12‰ change that is attributable to deep ocean circulation changes during this time interval, indicating a higher proportion of old, nutrient-rich waters (Pacific-like) during the LGM in this area, although productivity and air-sea gas exchange may also have contributed to this $\delta^{13}C$ variation. There are a number of $\delta^{13}C$ compilations for longer periods of time, including the most recent one by *Oliver et al*. [2010] for the last 150 ka B.P. The latter study documents similarly heavier values for interglacial MIS 1 and 5, lighter values for glacial MIS 2, and the lightest ones for MIS 6, reaching $\delta^{13}C$ signatures of *Cibicidoides* as low as −0.6. The authors assigned most of the glacial-interglacial variation to changes in carbon storage in the biosphere on land and also inferred modulations by changes in ocean circulation, productivity, and air-sea gas exchange. Figure 8 compares the benthic $\delta^{13}C$ data from our study (Core 59) to records from the central and western South Pacific [*Ninnemann and Charles*, 2002; *Elderfield et al*., 2012], the central equatorial Pacific [*Mix*, 1995], and the equatorial Indian Ocean [*Piotrowski et al*., 2009]. The variations in benthic carbon isotopes of Core 59 are very similar to those observed in other locations of the Pacific and even the interior of the Indian Ocean, further supporting a dominant role of terrestrial-oceanic carbon transfer in modulating the $\delta^{13}C$ variations. Only E11-2 differs from the other records in terms of absolute values, although the amplitude of glacial-interglacial change is very similar. Importantly, these data also confirm the absence of any significant effects of bioturbation on the amplitude and timing of any of the proxies measured in this study. The offset during sub-MIS 7d (~230 ka B.P. and ~220 ka B.P.) between Core 59 and the other records may originate from local productivity changes, but additional data would be needed to unambiguously confirm this.

4.3. Changes in the Detrital Provenance

Using combined Nd-Sr isotope compositions of the lithogenic fraction of the surface sediments, *Molina-Kescher et al*. [2014b] provided evidence on the provenance of the detrital, mainly eolian transported material, arriving at present in the South Pacific along ~40°S. On that study, the Nd-Sr isotope signatures

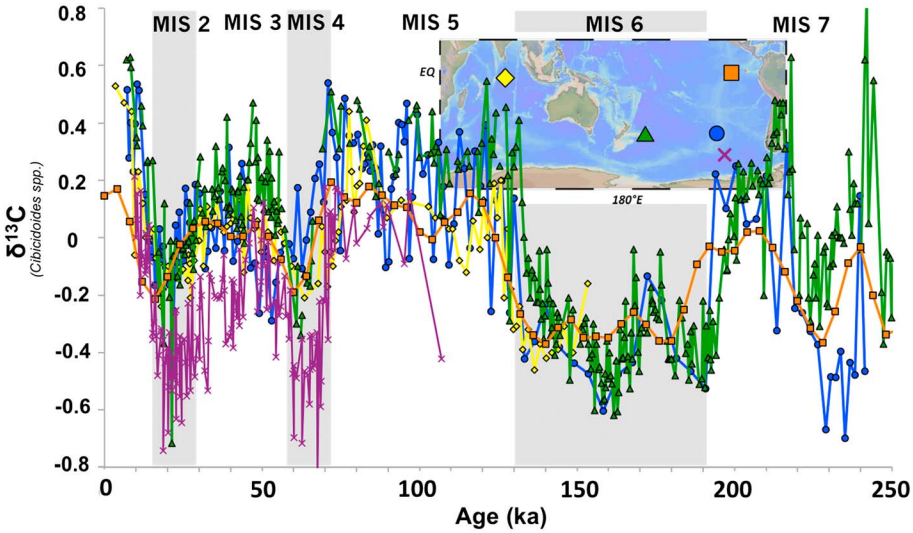

Figure 8. Comparison of benthic $\delta^{13}C$ records from comparable water depths in the Indian Ocean and the Pacific covering similar time scales. Yellow: core SK129-CR2 from 3800 m water depth [*Piotrowski et al*., 2009]; green: Ocean Drilling Program (ODP) Site 1123 from 3290 m water depth [*Elderfield et al*., 2012]; blue: core SO213-59-2 from 3161 m water depth (this study); purple: E11-2 from 3094 m water depth [*Ninnemann and Charles*, 2002]; and orange: ODP Site 849 from 3851 m water depth [*Mix*, 1995]. Shaded areas define full glacial marine isotope stages (MIS).

of the surface sediments from the Holocene and LGM (^{14}C ages ranging 5 to 24 ka B.P.) fall onto a trend line between the volcanic Andean rocks of South America, which dominate the Chile Basin, and the diverse lithologies of Australia and South New Zealand (see inset in Figure 9), which dominate west of ~110°W and reflects dust contributions transported by the dominant westerly winds (Figure 9) (see details in *Molina-Kescher et al*.,

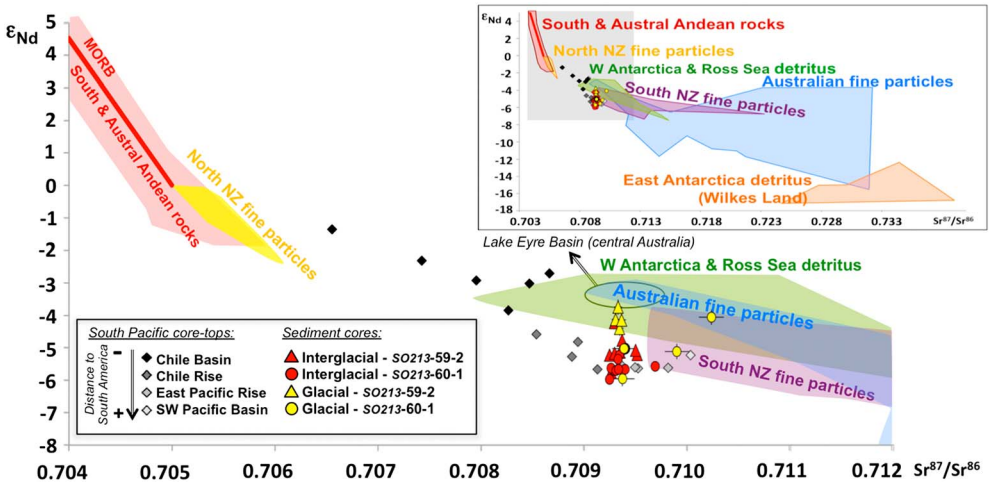

Figure 9. The role of different lithogenic sources contributing to the radiogenic Nd-Sr signal of detrital silicates of the South Pacific. Combined Nd and Sr isotope signatures of South Pacific core top and downcore detrital analyses are presented. The radiogenic isotope signatures of cores SO213-59-2 (triangles) and SO213-60-1 (circles) are separated into glacial (yellow) and interglacial (red) periods. The core top data from the open South Pacific (diamonds) [*Molina-Kescher et al*., 2014b] are given in black to light grey as a function of the distance to South America (see legend in the figure). The most probable detrital sources that surround the South Pacific are indicated as colored Sr-Nd isotope arrays: red: South Andean [*Hickey et al*., 1986; *Futa and Stern*, 1988] and Austral Andean rocks [*Futa and Stern*, 1988; *Stern and Kilian*, 1996]. Fine-grained particles (<5 μm) susceptible to eolian transport: yellow: North Island of New Zealand [*Delmonte et al*., 2004]; purple: South Island of New Zealand [*Taylor et al*., 1983; *Delmonte et al*., 2004]; blue: eastern Australia, whereby the Lake Eyre Basin is indicated by a circle [*Revel-Rolland et al*., 2006]; green: West Antarctic and Ross Sea detritus (combined from *Roy et al*. [2007] and *Hemming et al*. [2007]); and orange: Circum-Antarctic detritus from Wilkes Land (see inset) (combined from *Roy et al*. [2007] and *Hemming et al*. [2007]). MORB stands for Mid-Ocean Ridge Basalts. Note that the inset shows a larger range of potential source areas for Nd-Sr isotopes. The grey square marks the range of the large diagram.

[2014b]. Grain size sorting can cause fractionation of Sr isotopes [*Innocent et al*., 2000; *Tütken et al*., 2002], and the long distance of the closest continents to the two cores presented in this study only allows fine-grain detrital silicates to reach the study area. However, Nd isotopes are not significantly affected by grain size effects, and as *Molina-Kescher et al*. [2014b] demonstrated, the close correlation between Nd and Sr isotope compositions of the core top detrital silicates along a transect with increasing distance from the continental sources essentially excludes grain size sorting as the main controlling factor of the detrital Sr isotope variations of this region. We cannot exclude though that two small detrital radiogenic Sr isotope peaks of Core 60 were caused by short-term supply of finer-grained material. Therefore, the Nd-Sr isotope variability of the detrital material in Cores 59 and 60 provides information on past changes in the supply and provenance of the dust during the last ~240 ka B.P. although some Nd-Sr isotope fields of the source regions partly overlap. The interglacial data (red in Figure 9) closely match the Nd-Sr isotope signatures of the early Holocene core top samples (8–11 ka B.P.) obtained on the East Pacific Rise [*Molina-Kescher et al*., 2014b], indicating the dominance of the westerly winds carrying dust mainly from Australia and South New Zealand to the central South Pacific during warm periods [e.g., *Albani et al*., 2012; *Lamy et al*., 2014]. On the other hand, the glacial signatures are shifted toward more positive ε_{Nd} values and in the case of Core 60 also show more positive Sr isotope ratios, which are shifted toward the arrays of South New Zealand and Australian fine sediments of fluvioglacial origin and loess (blue and purple fields in Figure 9), which partially overlap with Nd-Sr isotope signatures from West Antarctica and detritus from the Ross Sea (green field in Figure 9). Due to the predominantly eastward directed water flow and wind pathways in these latitudes, these results clearly exclude any increase in glacial supply of material from South America to the open South Pacific. Ice-rafted debris was not found in either of the two investigated cores, essentially excluding icebergs as a significant means of transport. *Chase et al*. [2003] observed enhanced glacial supply of detrital material north of 66°S in the South Pacific, which they attributed to increased amounts of suspended load transported by the CDW to the central South Pacific, similar to observations in the South Atlantic, for which *Franzese et al*. [2006] and *Noble et al*. [2012] proposed that the ACC was more sediment laden during the LGM. This was likely originating from the stronger winds and larger sediment source areas during the LGM due to expanded deserts (consequence of a reduced hydrological cycle), lower sea level and enhanced exposure of shelf sediments, formation of mobile outwash plains from glaciers, and increased supply of glaciogenic debris by expanded ice sheets [*Noble et al*., 2012, and references therein], which led to the release of fine-grained weathered material to the Southern Ocean. Therefore, changes in the proportions of source regions of eolian inputs can explain the observed variations. A recent comprehensive study by *Lamy et al*. [2014], covering an extensive area of the Southern Ocean to the south of our location, supported the predominant eolian origin of lithogenic material accumulated in the sediments of the Pacific sector of the Southern Ocean and demonstrated a threefold increase in deposition of dust in the Pacific sector of the Southern Ocean during glacial periods of the past 1 Ma, consistently with enhanced westerly winds [e.g., *Albani et al*., 2012]. Although *Lamy et al*. [2014] inferred the dust to be derived from Australia and New Zealand, they did not provide any data on the provenance of the detrital material. Our data support their suggestions on the origin of the dust, and one possible explanation for the shift toward more positive Nd and Sr isotope signatures during glacial periods observed in this study may have been a stronger dust input from the region of the Lake Eyre Basin, central Australia. This potential source area (see inset in Figure 9) is characterized by a narrowly defined Nd-Sr isotopic field of ~−3 and ~0.7095, respectively [*Revel-Rolland et al*., 2006] and is less dependant on changes in rainfall than other contributing regions of Australia, such as the Murray-Darling River Basins (SE Australia) [*Revel-Rolland et al*., 2006]. This either reflects drier conditions in continental Australia or enhanced atmospheric transport due to higher wind speeds or a combination of both during glacials [e.g., *Hesse*, 1994].

5. Conclusions

The results of our study based on two sediment cores from the central South Pacific indicate a reduction of NADW admixture to the Southern Ocean during glacial stages supporting previous results from the southern Atlantic, Indian, and westernmost South Pacific. The deep water circulation proxies used in this study (Nd and Pb isotopes) show small but consistent variations: More radiogenic Nd and Pb isotopic signatures of deep waters prevailed during glacials, which is consistent with a similar reduction in the contribution of the least radiogenic end-member (NADW) to CDW during the LGM and MIS 6. Accordingly, CDW has prevailed in the

midlatitude (~45°S) central South Pacific at 3000/3500 m water depth during glacials. The small amplitude of the observed Nd and Pb isotope variability is consistent with the expected dilution of NADW along the flow path of CDW in the central South Pacific via mixing with Southern Ocean and Pacific waters.

Combined detrital Nd-Sr isotope compositions indicate that the provenance of lithogenic material arriving in the central South Pacific during the past ~240 ka B.P. remained stable in that Australian and New Zealand dust has remained the main source of continent-derived material brought to our study region by the dominant westerlies. However, the glacial signatures were shifted toward more radiogenic isotope compositions suggesting markedly increased contributions from regions with higher proportions of mantle-derived rock, such as the Lake Eyre region (central Australia). Detritus from Antarctica might have also reached the locations of our cores as suspended load of oceanic currents during glacials as a consequence of enhanced erosion and weathering inputs from the larger ice sheets.

Acknowledgments
We would like to thank the "Bundesministerium für Bildung und Forschung, Germany" for funding the collaborative research project SOPATRA (South Paleoceanographic Transects, 03G0213A and 03G0213B) jointly accomplished by GEOMAR and the Alfred Wegener Institute (AWI). We also thank the captain and crew of German R/V *Sonne* and participants of the expedition SO213, Ingmar Schindlbeck for lab support, and Editors Ellen Thomas and Christopher Charles. Comments by the latter, Taryn Noble, and an anonymous reviewer improved the quality of this paper. All results presented in this study are available at the PANGAEA® database (www.pangaea.de).

References

Abbot, A. N., B. A. Haley, J. McManus, and C. E. Reimers (2015a), The sedimentary flux of rare earth elements to the ocean, *Geochim. Cosmochim. Acta*, *154*, 186–200, doi:10.1016/j.gca.2015.01.010.

Abbot, A. N., B. A. Haley, and J. McManus (2015b), Bottoms up: Sedimentary control of the deep North Pacific Ocean's ε_{Nd} signature, *Geology*, doi:10.1130/G37114.1.

Abouchami, W., and S. L. Goldstein (1995), A lead isotopic study of Circum-Antarctic manganese nodules, *Geochim. Cosmochim. Acta*, *59*, 1809–1820.

Abouchami, W., S. J. G. Galer, and A. Koschinski (1999), Pb and Nd isotopes in NE Atlantic Fe–Mn crusts: Proxies for trace metal paleosources and paleocean circulation, *Geochim. Cosmochim. Acta*, *63*(10), 1489–1505.

Adkins, J. F. (2013), The role of deep ocean circulation in setting glacial climates, *Paleoceanography*, *28*, 539–561, doi:10.1002/palo.20046.

Albani, S., N. M. Mahowald, B. Delmonte, V. Maggi, and G. Winckler (2012), Comparing modeled and observed changes in mineral dust transport and deposition to Antarctica between the Last Glacial Maximum and current climates, *Clim. Dyn.*, *38*, 1731–1755.

Albarède, F., P. Telouk, J. Blichert-Toft, M. Boyet, A. Agranier, and B. Nelson (2004), Precise and accurate isotopic measurements using multiple-collector ICPMS, *Geochim. Cosmochim. Acta*, *68*(12), 2725–2744.

Amakawa, H., Y. Nozaki, D. S. Alibo, J. Zhang, K. Fukugawa, and H. Nagai (2004), Neodymium isotopic variations in Northwest Pacific water, *Geochim. Cosmochim. Acta*, *68*, 715–727.

Amakawa, H., K. Sasaki, and M. Ebihara (2009), Nd isotopic composition in the central North Pacific, *Geochim. Cosmochim. Acta*, *73*(16), 4705–4719.

Arsouze, T., J.-C. Dutay, F. Lacan, and C. Jeandel (2009), Reconstructing the Nd oceanic cycle using a coupled dynamical biogeochemical model, *Biogeosciences*, *6*(12), 2829–2846.

Barrat, J. A., F. Keller, J. Amosse, R. N. Taylor, R. W. Nesbitt, and T. Hirata (1996), Determination of rare earth elements in sixteen silicate reference samples by ICP-MS after Tm addition and ion exchange separation, *Geostand. Geoanal. Res.*, *20*, 133–139.

Basak, C., K. Pahnke, M. Frank, F. Lamy, and R. Gersonde (2015), Neodymium isotope characterization of Ross Sea Bottom Water and its advection through the southern South Pacific, *Earth Planet. Sci. Lett.*, *419*, 211–221.

Böhm, E., J. Lippold, M. Gutjahr, M. Frank, P. Blaser, B. Antz, J. Fohlmeister, N. Frank, M. Andersen, and M. Deininger (2015), Strong and deep Atlantic Meridional Overturning Circulation during the last glacial cycle, *Nature*, *517*, 73–76.

Boyle, E. A., and L. D. Keigwin (1986), Comparison of Atlantic and Pacific paleochemical records for the last 215,000 years: Changes in deep ocean circulation and chemical inventories, *Earth Planet. Sci. Lett.*, *76*(1–2), 135–150.

Broecker, W. S. (1982), Ocean chemistry during glacial time, *Geochim. Cosmochim. Acta*, *46*, 1689–1705.

Carter, L., I. N. McCave, and J. M. Williams (2009), Circulation and water masses of the Southern Ocean: A review, in *Developments in Earth and Environmental Sciences*, vol. 8, edited by F. Florindo and M. Siegert, pp. 85–114, Antarctic Climate Evolution, Elsevier, Netherlands.

Carter, P., D. Vance, C. D. Hillenbrand, J. A. Smith, and D. R. Shoosmith (2012), The neodymium isotopic composition of waters masses in the eastern Pacific sector of the Southern Ocean, *Geochim. Cosmochim. Acta*, *79*, 41–59.

Charles, C. D., and R. G. Fairbanks (1992), Evidence from Southern Ocean sediments for the effect of North Atlantic Deep Water flux on climate, *Nature*, *355*, 416–419.

Charles, C. D., J. D. Wright, and R. G. Fairbanks (1993), Thermodynamic influences on the marine carbon isotope record, *Paleoceanography*, *8*(6), 691–698, doi:10.1029/93PA01803.

Chase, Z., R. F. Anderson, M. Q. Fleisher, and P. W. Kubik (2003), Accumulation of biogenic and lithogenic material in the Pacific sector of the Southern Ocean during the past 40,000 years, *Deep Sea Res., Part II*, *50*, 799–832.

Chavagnac, V., M. R. Palmer, A. J. Milton, D. R. H. Green, and C. R. German (2006), Hydrothermal sediments as a potential record of seawater Nd isotope compositions: The Rainbow vent site (36°14′N, Mid-Atlantic Ridge), *Paleoceanography*, *21*, PA3012, doi:10.1029/2006PA001273.

Chow, T. J., and C. C. Patterson (1959), Lead isotopes in manganese nodules, *Geochim. Cosmochim. Acta*, *17*, 21–31.

Chow, T. J., and C. C. Patterson (1962), The occurrence and significance of lead isotopes in pelagic sediments, *Geochim. Cosmochim. Acta*, *26*, 263–308.

Crocket, K. C., D. Vance, G. L. Foster, D. A. Richards, and M. Tranter (2012), Continental weathering fluxes during the last glacial/interglacial cycle: Insights from the marine sedimentary Pb isotope record at Orphan Knoll, NW Atlantic, *Quat. Sci. Rev.*, *38*, 89–99.

Curry, W. B., and D. W. Oppo (2005), Glacial water mass geometry and the distribution of $\delta^{13}C$ of $\sum CO_2$ in the western Atlantic Ocean, *Paleoceanography*, *20*, PA1017, doi:10.1029/2004PA001021.

Delmonte, B., I. Basile-Doelsch, J.-R. Petit, V. Maggi, M. Revel-Rolland, A. Michard, E. Jagoutz, and F. Grousset (2004), Comparing the Epica and Vostok dust records during the last 220,000 years: Stratigraphical correlation and provenance in glacial periods, *Earth Sci. Rev.*, *66*, 63–87.

Duplessy, J.-C., N. J. Shackleton, R. G. Fairbanks, L. Labeyrie, D. W. Oppo, and N. Kallel (1988), Deepwater source variations during the last climatic cycle and their impact on the global deepwater circulation, *Paleoceanography*, *3*, 343–360, doi:10.1029/PA003i003p00343.

Elderfield, H., P. Ferretti, M. Greaves, S. Crowhurst, I. N. McCave, D. Hodell, and A. M. Piotrowski (2012), Evolution of ocean temperature and ice volume through the Mid-Pleistocene Climate Transition, *Science*, *337*(6095), 704–709.

Elmore, A. C., A. M. Piotrowski, J. D. Wright, and A. E. Scrivner (2011), Testing the extraction of past seawater Nd isotopic composition from North Atlantic marine sediments, *Geochem. Geophys. Geosyst.*, *12*, Q09008, doi:10.1029/2011GC003741.
Ferrari, R., M. F. Jansen, J. F. Adkins, A. Burke, A. L. Stewart, and A. F. Thompson (2014), Antarctic sea ice control on ocean circulation in present and glacial climates, *Proc. Natl. Acad. Sci. U. S. A.*, *111*(24), 8753–8758.
Foster, G. L., and D. Vance (2006), Negligible glacial–interglacial variation in continental chemical weathering rates, *Nature*, *444*, 918–921.
Frank M. (2002), Radiogenic isotopes: Tracers of past ocean circulation and erosional input, *Rev. Geophys.*, *40*(1), 1001, doi:10.1029/2000RG000094.
Franzese, A. M., S. R. Hemming, S. L. Goldstein, and R. F. Anderson (2006), Reduced Agulhas leakage at the LGM inferred from an integrated provenance and flux study, *Earth Planet. Sci. Lett.*, *250*, 72–88.
Futa, K., and C. R. Stern (1988), Sr and Nd isotopic and trace element compositions of Quaternary volcanic centers of the southern Andes, *Earth Planet. Sci. Lett.*, *88*, 253–262.
Galer, S. J. G., and R. K. O'Nions (1989), Chemical and isotopic studies of ultramafic inclusions from the San Carlos volcanic field, Arizona: A bearing on their petrogenesis, *J. Petrol.*, *30*(4), 1033–1064.
Garcia-Solsona, E., C. Jeandel, M. Labatut, F. Lacan, D. Vance, V. Chavagnac, and C. Pradoux (2014), Rare earth elements and Nd isotopes tracing water mass mixing and particle-seawater interactions in the SE Atlantic, *Geochim. Cosmochim. Acta*, *125*, 351–372.
Gebbie, G. (2014), How much did Glacial North Atlantic Water shoal?, *Paleoceanography*, *29*, 190–209, doi:10.1002/2013PA002557.
German, C. R., G. P. Klinkhammer, J. M. Edmond, A. Mitra, and H. Elderfield (1990), Hydrothermal scavenging of rare-earth elements in the ocean, *Nature*, *345*, 516–518.
Gooday, A. J. (2003), Benthic foraminifera (Protista) as tools in deep-water palaeoceanography: Environmental influences on faunal characteristics, *Adv. Mar. Biol.*, *46*, 3–70.
Gordon, A. L. (1975), An Antarctic oceanographic section along 170°E, *Deep Sea Res.*, *22*, 357–377.
Grasse, P., T. Stichel, R. Stumpf, L. Stramma, and M. Frank (2012), The distribution of neodymium isotopes and concentrations in the Eastern Equatorial Pacific: Water mass advection versus particle exchange, *Earth Planet. Sci. Lett.*, *353–354*, 198–207.
Gutjahr, M., M. Frank, C. H. Stirling, V. Klemm, T. van de Flierdt, and A. N. Halliday (2007), Reliable extraction of a deepwater trace metal isotope signal from Fe-Mn oxyhydroxide coatings of marine sediments, *Chem. Geol.*, *242*, 351–370.
Gutjahr, M., M. Frank, C. H. Stirling, L. D. Keigwin, and A. N. Halliday (2008), Tracing the Nd isotope evolution of North Atlantic Deep and Intermediate Waters in the western North Atlantic since the Last Glacial Maximum from Blake Ridge sediments, *Earth Planet. Sci. Lett.*, *266*, 61–77.
Gutjahr, M., M. Frank, A. N. Halliday, and L. D. Keigwin (2009), Retreat of the Laurentide ice sheet tracked by the isotopic composition of Pb in western North Atlantic seawater during termination 1, *Earth Planet. Sci. Lett.*, *286*, 546–555.
Haley, B. A., G. P. Klinkhammer, and J. McManus (2004), Rare earth elements in pore waters of marine sediments, *Geochim. Cosmochim. Acta*, *68*, 1265–1279, doi:10.1016/j.gca.2003.09.012.
Halliday, A. N., J. P. Davidson, P. Holden, R. M. Owen, and A. M. Olivarez (1992), Metalliferous sediments and the scavenging residence time of Nd near hydrothermal vents, *Geophys. Res. Lett.*, *19*, 761–764, doi:10.1029/92GL00393.
Hemming, S. R., T. van de Flierdt, S. L. Goldstein, A. M. Franzese, M. Roy, G. Gastineu, and G. Landrot (2007), Strontium isotope tracing of terrigenous sediment dispersal in the Antarctic Circumpolar Current: Implications for constraining frontal positions, *Geochem. Geophys. Geosyst.*, *8*, Q06N13, doi:10.1029/2006GC001441.
Hesse, P. P. (1994), The record of continental dust from Australia in Tasman Sea sediments, *Quat. Sci. Rev.*, *13*, 257–272.
Hickey, R. L., F. A. Frey, and D. C. Gerlach (1986), Multiple sources for basaltic arc rocks from the Southern Volcanic Zone of the Andes (34°–41°S): Trace element and isotopic evidence for contributions from subducted oceanic crust, mantle and continental crust, *J. Geophys. Res.*, *91*, 5963–5983, doi:10.1029/JB091iB06p05963.
Horikawa, K., E. E. Martin, Y. Asahara, and T. Sagawa (2011), Limits on conservative behavior of Nd isotopes in seawater assessed from analysis of fish teeth from Pacific core tops, *Earth Planet. Sci. Lett.*, *310*, 119–130.
Horwitz, E. P., R. Chiarizia, and M. L. Dietz (1992), A novel strontium-selective extraction chromatographic resin, *Solvent Extr. Ion Exch.*, *10*, 313–336.
Huang, K.-F., C.-F. You, C.-H. Chung, Y.-H. Lin, and Z. Liu (2014), Tracing the Nd isotope evolution of North Pacific Intermediate and Deep Waters through the last deglaciation from South China Sea sediments, *J. Asian Earth Sci.*, *79*, 564–573.
Innocent, C., N. Fagel, and C. Hillaire-Marcel (2000), Sm-Nd isotope systematics in deep-sea sediments: Clay-size versus coarser fractions, *Mar. Geol.*, *168*, 79–87.
Jacobsen, S. B., and G. J. Wasserburg (1980), Sm–Nd isotopic evolution of chondrites, *Earth Planet. Sci. Lett.*, *50*, 139–155.
Jeandel, C., T. Arsouze, F. Lacan, P. Techine, and J. C. Dutay (2007), Isotopic Nd compositions and concentrations of the lithogenic inputs into the ocean: A compilation, with an emphasis on the margins, *Chem. Geol.*, *239*, 156–164.
Kawabe, M., and S. Fujio (2010), Pacific Ocean circulation based on observation, *J. Oceanogr.*, *66*, 389–403.
Keigwin, L. D. (1998), Glacial-age hydrography of the northwest Pacific Ocean, *Paleoceanography*, *13*(4), 323–339, doi:10.1029/98PA00874.
Kraft, S., M. Frank, E. C. Hathorne, and S. Weldeab (2013), Assessment of seawater Nd isotope signatures extracted from foraminiferal shells and authigenic phases of Gulf of Guinea sediments, *Geochim. Cosmochim. Acta*, *121*, 414–435.
Lacan, F., and C. Jeandel (2005), Neodymium isotopes as a new tool for quantifying exchange fluxes at the continent-ocean interface, *Earth Planet. Sci. Lett.*, *232*, 245–257.
Lambelet, M., T. van de Flierdt, K. Crocket, M. Rehkämper, K. Kreissig, B. Coles, M. J. A. Rijkenberg, L. J. A. Gerringa, H. J. W. de Baar, and R. Steinfeldt (2016), Neodymium isotopic composition and concentration in the western North Atlantic Ocean: Results from the GEOTRACES GA02 section, *Geochim. Cosmochim. Acta*, *177*, 1–29, doi:10.1016/j.gca.2015.12.019.
Lamy, F., R. Gersonde, G. Winckler, O. Esper, A. Jaeschke, G. Kuhn, J. Ullermann, A. Martinez-Garcia, F. Lambert, and R. Kilian (2014), Increased dust deposition in the Pacific Southern Ocean during glacial periods, *Science*, *343*, 403.
Le Fevre, B., and C. Pin (2005), A straightforward separation scheme for concomitant Lu–Hf and Sm–Nd isotope ratio and isotope dilution analysis, *Anal. Chim. Acta*, *543*, 209–221.
Lisiecki, L. E., and M. E. Raymo (2005), A Pliocene-Pleistocene stack of 57 globally distributed benthic $\delta^{18}O$ records, *Paleoceanography*, *20*, PA1003, doi:10.1029/2004PA001071.
Lugmair, G. W., and S. J. G. Galer (1992), Age and isotopic relationships among the angrites Lewis Cliff 86010 and Angra dos Reis, *Geochim. Cosmochim. Acta*, *56*, 1673–1694.
Lynch-Stieglitz, J. (2003), Tracers of past ocean circulation, in *Treatise on Geochemistry*, vol. 6, edited by H. D. Holland and K. K. Turekian, pp. 433–451, Elsevier, Oxford, U. K.
Mackensen, A., H. W. Hubberten, T. Bickert, G. Fischer, and D. K. Futterer (1993), The $\delta^{13}C$ in benthic foraminiferal tests of *Fontbotia wuellerstorfi* (Schwager) relative to the $\delta^{13}C$ of dissolved inorganic carbon in Southern Ocean deep water: Implications for glacial ocean circulation models, *Paleoceanography*, *8*, 587–610, doi:10.1029/93PA01291.

Martin, E. E., and H. D. Scher (2004), Preservation of seawater Sr and Nd isotopes in fossil fish teeth: Bad news and good news, *Earth Planet. Sci. Lett.*, *220*, 25–39.
Matsumoto, K., and J. Lynch-Stieglitz (1999), Similar glacial and Holocene deepwater circulation inferred from southeast Pacific benthic foraminiferal carbon isotope composition, *Paleoceanography*, *14*(2), 149–163, doi:10.1029/1998PA900028.
Matsumoto, K., T. Oba, J. Lynch-Stieglitz, and H. Yamamoto (2002), Interior hydrography and circulation of the glacial Pacific Ocean, *Quat. Sci. Rev.*, *21*, 1693–1704.
McCave, I. N., L. Carter, and I. R. Hall (2008), Glacial–interglacial changes in water mass structure and flow in the SW Pacific Ocean, *Quat. Sci. Rev.*, *27*, 1886–1908.
McManus, J. F., R. Francois, J.-M. Gherardi, L. Keigwin, and S. Brown-Leger (2004), Collapse and rapid resumption of Atlantic meridional circulation linked to deglacial climate changes, *Nature*, *428*, 834–837.
Mix, A. C. (1995), Benthic foraminifer stable isotope record from Site 849 (0–5 Ma): Local and global climate changes, *Proc. Ocean Drill. Program Sci. Results*, *138*, 371–412.
Molina-Kescher, M., M. Frank, and E. Hathorne (2014a), South Pacific dissolved Nd isotope compositions and rare earth element distributions: Water mass mixing versus biogeochemical cycling, *Geochim. Cosmochim. Acta*, *127*, 171–189.
Molina-Kescher, M., M. Frank, and E. C. Hathorne (2014b), Nd and Sr isotope compositions of different phases of surface sediments in the South Pacific: Extraction of seawater signatures, boundary exchange, and detrital/dust provenance, *Geochem. Geophys. Geosyst.*, *15*, 3502–3520, doi:10.1002/2014GC005443.
Ninnemann, U. S., and C. D. Charles (2002), Changes in the mode of Southern Ocean circulation over the last glacial cycle revealed by foraminiferal stable isotopic variability, *Earth Planet. Sci. Lett.*, *201*(2), 383.
Noble, T. L., A. M. Piotrowski, L. F. Robinson, J. F. McManus, C.-D. Hillenbrand, and A. J.-M. Bory (2012), Greater supply of Patagonian sourced detritus and transport by the ACC to the Atlantic sector of the Southern Ocean during the last glacial period, *Earth Planet. Sci. Lett.*, *317*, 374–385.
Noble, T. L., A. M. Piotrowski, and I. N. McCave (2013), Neodymium isotopic composition of intermediate and deep waters in the glacial southwest Pacific, *Earth Planet. Sci. Lett.*, *384*, 27–36.
Oliver, K. I. C., B. A. A. Hoogakker, S. Crowhurst, G. M. Henderson, R. E. M. Rickaby, N. R. Edwards, and H. Elderfield (2010), A synthesis of marine sediment core $\delta^{13}C$ data over the last 150 000 years, *Clim. Past*, *6*, 645–673.
Orsi, A. H., G. C. Johnson, and J. L. Bullister (1999), Circulation, mixing, and production of Antarctic Bottom Water, *Prog. Oceanogr.*, *43*, 55–109.
Pearce, C. R., M. T. Jones, E. H. Oelkers, C. Pradoux, and C. Jeandel (2013), The effect of particulate dissolution on the neodymium (Nd) isotope and Rare Earth Element (REE) composition of seawater, *Earth Planet. Sci. Lett.*, *369-370*, 21–40.
Pena, L. D., and S. L. Goldstein (2014), Thermohaline circulation crisis and impacts during the mid-Pleistocene transition, *Science*, *345*(6194), 318–322.
Peterson, C. D., L. E. Lisiecki, and J. V. Stern (2014), Deglacial whole-ocean $\delta^{13}C$ change estimated from 480 benthic foraminiferal records, *Paleoceanography*, *29*, 549–563, doi:10.1002/2013PA002552.
Piepgras, D. J., and S. B. Jacobsen (1988), The isotopic composition of neodymium in the North Pacific, *Geochim. Cosmochim. Acta*, *52*, 1373–1381.
Piepgras, D. J., and G. J. Wasserburg (1982), Isotopic composition of neodymium in waters from the Drake Passage, *Science*, *217*, 207–214.
Piepgras, D. J., and G. J. Wasserburg (1987), Rare earth element transport in the western North Atlantic inferred from Nd isotopic observations, *Geochim. Cosmochim. Acta*, *51*, 1257–1271.
Piotrowski, A. M., S. L. Goldstein, S. R. Hemming, and R. G. Fairbanks (2004), Intensification and variability of ocean thermohaline circulation through the last deglaciation, *Earth Planet. Sci. Lett.*, *225*, 205–220.
Piotrowski, A. M., S. L. Goldstein, S. R. Hemming, and R. G. Fairbanks (2005), Temporal relationships of carbon cycling and ocean circulation at glacial boundaries, *Science*, *307*, 1933–1938.
Piotrowski, A. M., S. L. Goldstein, S. R. Hemming, R. G. Fairbanks, and D. R. Zylberberg (2008), Oscillating glacial northern and southern deep water formation from combined neodymium and carbon isotopes, *Earth Planet. Sci. Lett.*, *272*(1–2).
Piotrowski, A. M., V. K. Banakar, A. E. Scrivner, H. Elderfield, A. Galy, and A. Dennis (2009), Indian Ocean circulation and productivity during the last glacial cycle, *Earth Planet. Sci. Lett.*, *285*, 179–189.
Piotrowski, A. M., A. Galy, J. A. L. Nicholl, N. Roberts, D. J. Wilson, J. A. Clegg, and J. Yu (2012), Reconstructing deglacial North and South Atlantic deep water sourcing using foraminiferal Nd isotopes, *Earth Planet. Sci. Lett.*, *357-358*, 289–297.
Rahmstorf, S. (2002), Ocean circulation and climate during the past 120,000 years, *Nature*, *419*, 207–214.
Ravelo, A. C., and C. Hillaire-Marcel (2007), The use of oxygen and carbon isotopes of foraminifera in paleoceanography, in *Developments in Marine Geology: Proxies in Late Cenozoic Paleoceanography*, vol. 1, edited by C. Hillaire-Marcel and A. De Vernal, pp. 735–764, Elsevier, Amsterdam, Netherlands.
Reid, J. L. (1986), On the total geostrophic circulation of the South Pacific Ocean: Flow patterns, tracers and transports, *Prog. Oceanogr.*, *16*, 1–61.
Reid, J. L., and R. J. Lynn (1971), On the influence of the Norwegian-Greenland and Weddell seas upon the bottom waters of the Indian and Pacific oceans, *Deep Sea Res.*, *18*, 1063–1088.
Rempfer, J., T. F. Stocker, F. Joos, J. C. Dutay, and M. Siddall (2011), Modelling Nd isotopes with a coarse resolution ocean circulation model: Sensitivities to model parameters and source/sink distributions, *Geochim. Cosmochim. Acta*, *75*, 5927–5950.
Revel-Rolland, M., P. De Deckker, B. Delmonte, P. P. Hesse, J. W. Magee, I. Basile-Doelsch, F. Grousset, and D. Bosch (2006), Eastern Australia: A possible source of dust in East Antarctica interglacial ice, *Earth Planet. Sci. Lett.*, *249*, 1–13.
Rickli, J., M. Frank, and A. N. Halliday (2009), The hafnium neodymium isotopic composition of Atlantic seawater, *Earth Planet. Sci. Lett.*, *280*, 118–127.
Rickli, J., M. Gutjahr, D. Vance, M. Fischer-Gödde, C. D. Hillenbrand, and G. Kuhn (2014), Neodymium and hafnium boundary contributions to seawater along the West Antarctic continental margin, *Earth Planet. Sci. Lett.*, *394*, 99–110.
Roberts, N. L., A. M. Piotrowski, J. F. McManus, and L. D. Keigwin (2010), Synchronous deglacial overturning and water mass source changes, *Science*, *327*, 75–78.
Roberts, N. L., A. M. Piotrowski, H. Elderfield, T. I. Eglinton, and M. W. Lomas (2012), Rare earth element association with foraminifera, *Geochim. Cosmochim. Acta*, *94*, 57–71.
Robinson, L. F., and T. van de Flierdt (2009), Southern Ocean evidence for reduced export of North Atlantic DeepWater during Heinrich event 1, *Geology*, *37*(3), 195–198.
Roy, M., T. van de Flierdt, S. R. Hemming, and S. L. Goldstein (2007), $^{40}Ar/^{39}Ar$ ages of hornblende grains and bulk Sm/Nd isotopes of circum-Antarctic glacio-marine sediments: Implications for sediment provenance in the Southern Ocean, *Chem. Geol.*, *244*, 507–519.

Rutberg, R. L., S. R. Hemming, and S. L. Goldstein (2000), Reduced North Atlantic Deep Water flux to the glacial Southern Ocean inferred from neodymium isotope ratios, *Nature*, *405*, 935–938.
Sarnthein, M., K. Winn, S. J. A. Jung, J. C. Duplessy, L. Labeyrie, H. Erlenkeuser, and G. Ganssen (1994), Changes in East Atlantic Deepwater Circulation over the last 30,000 years: Eight time slice reconstructions, *Paleoceanography*, *9*, 209–267, doi:10.1029/93PA03301.
Schaule, B. K., and C. C. Patterson (1981), Lead concentrations in the north Pacific: Evidence for global anthropogenic perturbations, *Earth Planet. Sci. Lett.*, *54*, 97–116.
Sigman, D. M., M. P. Hain, and G. H. Haug (2010), The polar ocean and glacial cycles in atmospheric CO_2 concentration, *Nature*, *466*(7302), 47–55.
Singh, S. P., S. K. Singh, V. Goswami, R. Bhushan, and V. K. Rai (2012), Spatial distribution of dissolved neodymium and ε_{Nd} in the Bay of Bengal: Role of particulate matter and mixing of water masses, *Geochim. Cosmochim. Acta*, *94*, 38–56.
Stern, C. R., and R. Kilian (1996), Role of the subducted slab, mantle wedge and continental crust in the generation of adakites from the Andean Austral Volcanic Zone, *Contrib. Mineral. Petrol.*, *123*, 163–281.
Stichel, T., M. Frank, J. Rickli, and B. A. Haley (2012a), The hafnium and neodymium isotope composition of seawater in the Atlantic sector of the Southern Ocean, *Earth Planet. Sci. Lett.*, *317*, 282–294.
Stichel, T., M. Frank, J. Rickli, E. C. Hathorne, B. A. Haley, C. Jeandel, and C. Pradoux (2012b), Sources and input mechanisms of hafnium and neodymium in surface waters of the Atlantic sector of the Southern Ocean, *Geochim. Cosmochim. Acta*, *94*, 22–37.
Stumpf, R., M. Frank, J. Schönfeld, and B. A. Haley (2010), Late Quaternary variability of Mediterranean Outflow Water from radiogenic Nd and Pb isotopes, *Quat. Sci. Rev.*, *29*, 2462–2472.
Tachikawa K., V. Athias and C. Jeandel (2003), Neodymium budget in the modern ocean and paleo-oceanographic implications, *J. Geophys. Res.*, *108*(C8), 3254, doi:10.1029/1999JC000285.
Tachikawa, K., A. M. Piotrowski, and G. Bayon (2014), Neodymium associated with foraminiferal carbonate as a recorder of seawater isotopic signatures, *Quat. Sci. Rev.*, *88*, 1–13.
Tanaka, T., et al. (2000), JNdi-1: A neodymium isotopic reference in consistency with LaJolla neodymium, *Chem. Geol.*, *168*(3–4), 279–281.
Tapia, R., D. Nürnberg, T. Ronge, and R. Tiedemann (2015), Disparities in glacial advection of Southern Ocean Intermediate Water to the South Pacific Gyre, *Earth Planet. Sci. Lett.*, *410*, 152–164.
Taylor, S. R., S. M. McLennan, and M. T. McCulloch (1983), Geochemistry of loess, continental crustal composition and crustal model ages, *Geochim. Cosmochim. Acta*, *47*, 1897–1905.
Teschner, C., M. Frank, B. A. Haley, and J. Knies (2016), Plio-Pleistocene evolution of water mass exchange and erosional input at the Atlantic-Arctic gateway, *Paleoceanography*, *31*, doi:10.1002/2015PA002843.
Tiedemann R., F. Lamy, and cruise participants (2012), FS Sonne Fahrtbericht/Cruise Report SO213-SOPATRA: South Pacific Paleoceanographic Transects—Geodynamic and Climatic Variability in Space and Time, Leg 1: Valparaiso/Chile - Valparaiso/Chile, 27.012.2010 - 12.01.2011, Leg 2: Valparaiso/Chile - Wellington/New Zealand, 12.01.2011 - 07.03.2011. doi:10.2312/cr_so213.
Tütken, T., A. Eisenhauer, B. Wiegand, and B. T. Hansen (2002), Glacial–interglacial cycles in Sr and Nd isotopic composition of Arctic marine sediments triggered by the Svalbard/Barents Sea ice sheet, *Mar. Geol.*, *182*, 351–372.
van de Flierdt, T., L. F. Robinson, J. F. Adkins, S. R. Hemming, and S. L. Goldstein (2006), Temporal stability of the neodymium isotope signature of the Holocene to glacial North Atlantic, *Paleoceanography*, *21*, PA4102, doi:10.1029/2006PA001294.
van de Flierdt, T., S. L. Goldstein, S. R. Hemming, M. Roy, M. Frank, and A. N. Halliday (2007), Global neodymium-hafnium isotope systematics—Revisited, *Earth Planet. Sci. Lett.*, *259*, 432–441.
von Blanckenburg, F., and H. Igel (1999), Lateral mixing and advection of reactive isotopes in ocean basins: Observations and mechanisms, *Earth Planet. Sci. Lett.*, *169*, 113–128.
Warren, B. A. (1973), Transpacific hydrographic sections at latitudes 43°S and 28°S: The SCORPIO Expedition II. Deep Water, *Deep Sea Res.*, *20*, 9–38.
Wilson, D. J., A. M. Piotrowski, A. Galy, and J. A. Clegg (2013), Reactivity of neodymium carriers in deep sea sediments: Implications for boundary exchange on paleoceanography, *Geochim. Cosmochim. Acta*, *109*, 197–221.
Wilson, D. J., K. C. Crocket, T. van de Flierdt, L. F. Robinson, and J. F. Adkins (2014), Dynamic intermediate ocean circulation in the North Atlantic during Heinrich Stadial 1: A radiocarbon and neodymium isotope perspective, *Paleoceanography*, *29*, 1072–1093, doi:10.1002/2014PA002674.
Wilson, D. J., A. M. Piotrowski, A. Galy, and V. K. Banakar (2015a), Interhemispheric controls on deep ocean circulation and carbon chemistry during the last two glacial cycles, *Paleoceanography*, *30*, 621–641, doi:10.1002/2014PA002707.
Wilson, D. J., A. Galy, A. M. Piotrowski, and V. K. Banakar (2015b), Quaternary climate modulation of Pb isotopes in the deep Indian Ocean linked to the Himalayan chemical weathering, *Earth Planet. Sci. Lett.*, *424*, 256–268.